Title: Flexible coordinator and switcher hubs for adaptive task control

Abbreviated title: Flexible coordinator and switcher hubs

Authors: Carrisa V Cocuzza (corresponding author)[1,2], Takuya Ito[1,2], Douglas Schultz[1,3], Danielle S Bassett[4], Michael W Cole[1]

[1]Center for Molecular and Behavioral Neuroscience, Rutgers University, Newark, NJ, USA, 07102
[2]Behavioral and Neural Sciences PhD Program, Rutgers University, Newark, NJ, USA, 07102
[3]Center for Brain Biology and Behavior, University of Nebraska-Lincoln, Lincoln, NE, USA, 68588
[4]Departments of Bioengineering, Physics & Astronomy, Electrical & Systems Engineering, and Neurology, University of Pennsylvania, Philadelphia, PA, USA, 19104

Corresponding author:
Carrisa Cocuzza, Center for Molecular and Behavioral Neuroscience, Rutgers University
197 University Avenue, Newark, NJ 07102
carrisacocuzza@gmail.com

Conflict of Interest: The authors declare no competing financial interests.

Acknowledgments: This project was supported by the US National Institutes of Health, under awards K99-R00 MH096901 and R01 MH109520. The content is the sole responsibility of the authors and does not necessarily represent the official views of any of the funding agencies. The authors acknowledge the Office of Advanced Research Computing (OARC) at Rutgers, The State University of New Jersey for providing access to the Amarel cluster and associated research computing resources. The authors thank their colleagues at the Cole Neurocognition Lab and the Rutgers University Brain Imaging Center (RUBIC) for their expertise and diligent efforts in data collection, as well as offering words of wisdom and overall support.

Keywords: cognitive control, functional connectivity, network dynamics, executive function, cognitive flexibility

Abstract

Functional connectivity studies have identified at least two large-scale neural systems that constitute cognitive control networks – the frontoparietal network (FPN) and cingulo-opercular network (CON). Control networks are thought to support goal-directed cognition and behavior. It was previously shown that the FPN flexibly shifts its global connectivity pattern according to task goal, consistent with a "flexible hub" mechanism for cognitive control. Our aim was to build on this finding to develop a functional cartography (a multi-metric profile) of control networks in terms of dynamic network properties. We quantified network properties in (male and female) humans using a high-control-demand cognitive paradigm involving switching among 64 task sets. We hypothesized that cognitive control is enacted by the FPN and CON via distinct but complementary roles reflected in network dynamics. Consistent with a flexible "coordinator" mechanism, FPN connections were globally diverse across tasks, while maintaining within-network connectivity to aid cross-region coordination. Consistent with a flexible "switcher" mechanism, CON regions switched to other networks in a task-dependent manner, driven primarily by reduced within-network connections to other CON regions. This pattern of results suggests FPN acts as a dynamic, global coordinator of goal-relevant information, while CON transiently disbands to lend processing resources to other goal-relevant networks. This cartography of network dynamics reveals a dissociation between two prominent cognitive control networks, suggesting complementary mechanisms underlying goal-directed cognition.

Significance Statement

Cognitive control supports a variety of behaviors requiring flexible cognition, such as rapidly switching between tasks. Furthermore, cognitive control is negatively impacted in a variety of mental illnesses. We used tools from network science to characterize the implementation of cognitive control by large-scale brain systems. This revealed that two systems – the frontoparietal (FPN) and cingulo-opercular (CON) networks – have distinct but complementary roles in controlling global network reconfigurations. The FPN exhibited properties of a flexible coordinator (orchestrating task changes in a coordinated manner), while CON acted as a flexible switcher (switching specific regions to other systems to lend processing resources). These findings reveal an underlying distinction in cognitive processes that may be applicable to clinical, educational, and machine learning work targeting cognitive flexibility.

Introduction

Theories of cognitive control – processes supporting goal-directed cognition and behavior – suggest the need for flexibly reconfigurable systems to support controlled processing (Schneider and Shiffrin 1977; Schneider and Chein 2003; Cole et al. 2010 & 2013b). An individual's goals, environment, and state are all subject to change over time. To accord with these fluctuations, controlled processing must also be dynamic (Miller and Cohen 2001). Recent evidence suggests that control dynamics are neurally supported by network reconfigurations (Cole et al. 2013b). Moreover, multiple brain networks are proposed to enact controlled processing – collectively termed cognitive control networks (Dosenbach et al. 2007; Power et al. 2011).

Control networks are posited to include at least two large-scale systems – the frontoparietal network (FPN) and cingulo-opercular network (CON) (Dosenbach et al. 2008; Crittenden et al. 2016). Control networks have been described as "task-positive", demonstrating increased activity during goal-directed cognition (Fox et al. 2005; Cole and Schneider 2007). Specifically, FPN regions exhibit adaptive coding across a variety of task demands (Stokes et al. 2013), and top-down modulation of other brain regions (Hwang et al. 2017). However, functional characterization of the CON is less clear. Some studies

suggest that CON regions support sustained (tonic) alertness (Sadaghiani and D'Esposito 2015), and prolonged "task set maintenance" (Dosenbach et al. 2006 & 2007) . Others highlight CON's role in selective (phasic) attention (Seeley et al. 2007), especially in the presence of response conflict (Cole et al. 2009; Botvinick 2007). Collectively, it is also unclear if FPN and CON regions act in cooperation or competition (Cocchi et al. 2013). Thus, while considerable evidence suggests that FPN and CON regions support cognitive control, a clear functional dissociation between the two has not been established.

The goal of the present study is to apply network science tools to advance understanding of how FPN and CON implement controlled processing. Given the dynamic nature of control, we focused on changes in task-state functional connectivity (tFC) across multiple states, relative to resting-state functional connectivity (rsFC). Importantly, **while** tFC across many states closely resembles intrinsic rsFC (Cole et al. 2014; Krienen et al. 2014), slight reconfigurations from rsFC to tFC carry functionally meaningful changes that support the task at hand (Hearne et al. 2017; Cole et al. 2013b). Further, given that the more practiced one is at a given task the less they utilize control (Chein and Schneider 2012) we administered a rapid instructed task learning (RITL) cognitive paradigm involving many systematically-related novel tasks (Cole et al. 2010 & 2013a; Ito et al. 2017). This is called the Concrete Permuted Rule Operations (C-PRO; Fig. 1) paradigm, and was administered during collection of functional magnetic resonance imaging (fMRI) data. Resting-state fMRI scans were also obtained, allowing us to synthesize the benefits of a RITL paradigm with the observation that task states emerge out of an intrinsic state, and assess functional reconfigurations between states.

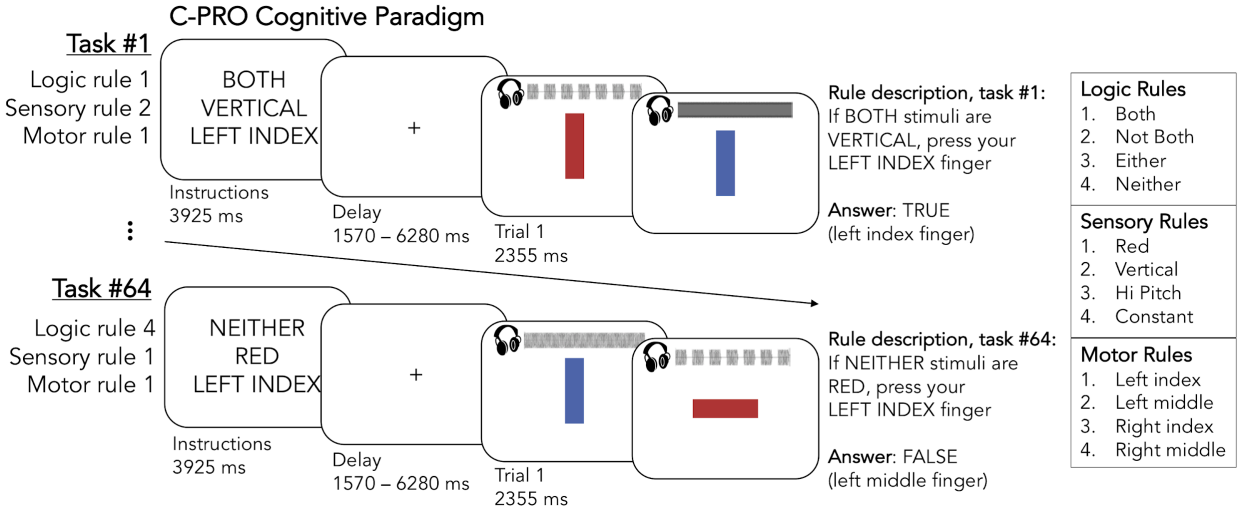

Figure 1. The Concrete Permuted Rule Operations (C-PRO) cognitive paradigm. First, an instruction screen presented the rules for a given task (3925 ms). Participants next applied these rules to pairs of consecutively presented audiovisual stimuli (auditory waveforms are visually depicted here, but were only presented audibly to participants). Two example task-rule sets are depicted, as well as how participants were trained to interpret the rules (e.g., rule descriptions on the right-most portion of panel A) (see Materials and Methods for details). The 12 possible rules are listed on the right.

To quantify cognitive changes across C-PRO task states, we employed a "network mechanism" approach that is thought to provide explanatory power to observed links between neural data and cognition via experimental manipulation of cognitive demands (Mill et al. 2017). Firstly, we quantified changes in connectivity across task states with network metrics (Fig. 2 & Table 1). Some of these metrics, such as global variability coefficient (GVC) and network flexibility (NF), have previously been linked with flexible network reconfiguration (Fig. 2A & 2B) (Cole et al. 2013; Bassett et al. 2011; 2013a; 2013b). However, mathematical principles and results of these existing graph metrics diverged. To reconcile this

in a principled manner, we developed a novel graph metric, network partition deviation (or just "deviation"), that generated quantitative profiles of network reassignments across states (Table 1, Fig. 2C). Secondly, we developed functional cartographies, or "maps", representing pivotal network properties across multiple continuous dimensions (Guimerà and Nunes Amaral 2005; Mattar et al. 2015).

We hypothesized that these cartographies would reveal dissociable and complementary cognitive control mechanisms for FPN and CON regions. Prior work suggested that FPN connections would dynamically reconfigure in a globally diverse manner (Cole et al. 2013b). Extrapolating from work emphasizing sustained task-related activity in CON (Dosenbach et al. 2006 & 2007; Sadaghiani and D'Esposito 2015), we hypothesized that CON connections would reconfigure consistently across states. Altogether, we hypothesized that FPN regions act as "flexible coordinators" and CON regions as "flexible switchers", both providing complementary functions in support of cognitive control.

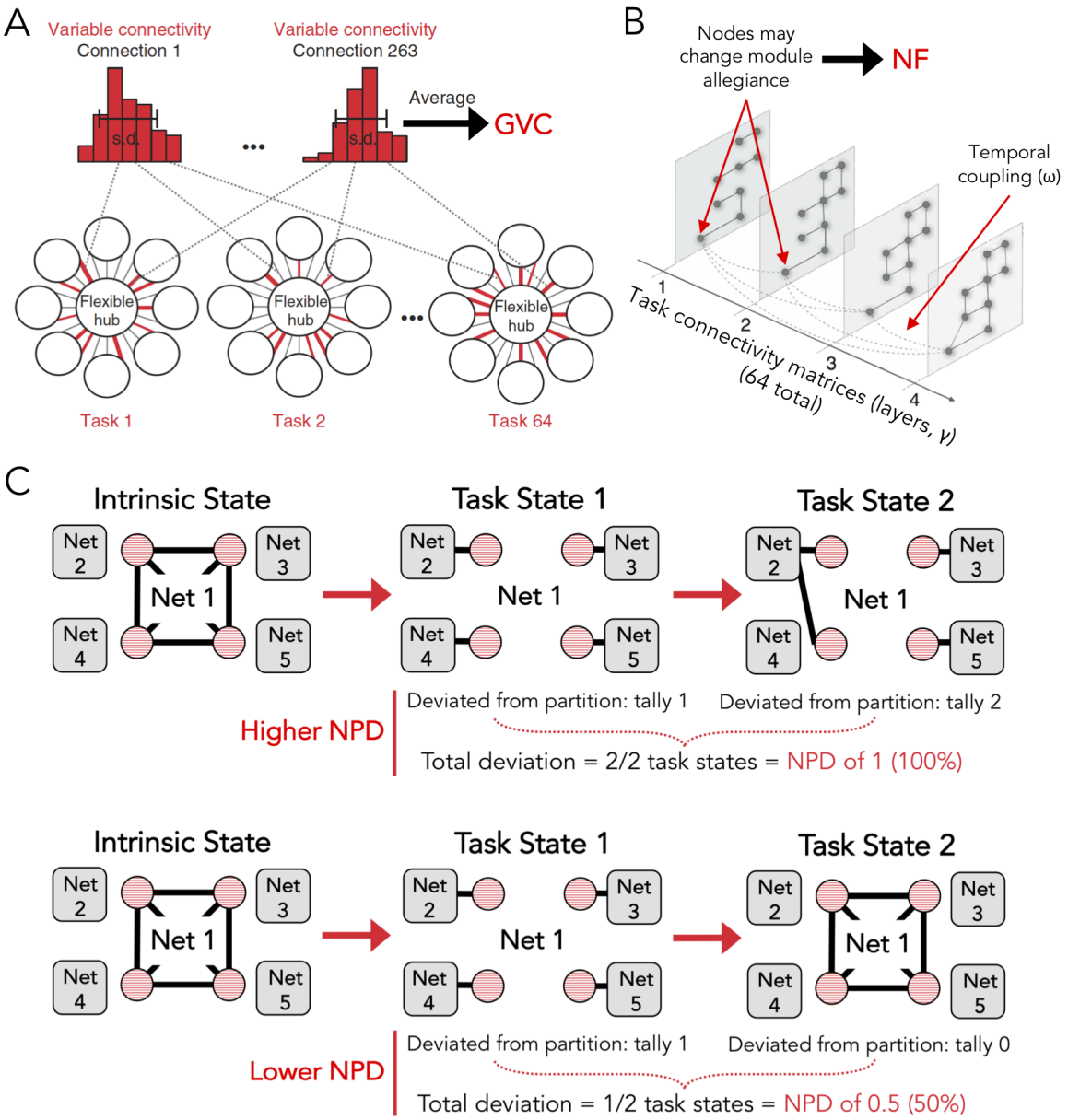

Figure 2. Schematic depictions of network metric algorithms. (***A***) Global variability coefficient (GVC), reproduced with permission (Cole et al. 2013b). Between-network variability coefficient (BVC) is measured equivalently, except within-network connections are withheld. (***B***) Network flexibility (NF), reproduced with permission (Cole et al. 2014; Bassett et al. 2013a; Mucha et al. 2010). Task connectivity matrices (layers) are passed through a multilayer community detection algorithm that accepts spatial and temporal resolution parameters (γ and ω, respectively). Resulting community assignments are assessed for "module allegiance" across states. Less allegiance results in higher NF. (***C***) Network partition deviation. Connectivity-based network "preferences" are tallied across task states, and how often a given network (Net 1) deviates from its predefined partition is computed [tally / total number of tasks]. In the example of higher deviation, Net 1 deviates in two out of two hypothetical states (100% deviation=deviation of 1.0). In the example of lower deviation, Net 1 deviates in one out of two hypothetical task states (50% deviation=deviation of 0.5).

Table 1. Graph theoretical diagnostic metrics for network reconfiguration properties across states.

Metric name	Formula	Measures; Diagnoses	Parameter-space?	Relies on a pre-defined partition?
Global Variability Coefficient (GVC)	$GVC_n = \frac{1}{N}\sum_{i=1}^{n}\sqrt{\frac{\sum_{l=1}^{T}(FC_{il} - \bar{x}_{FCl})^2}{T-1}}$	Variable FC across tasks; flexible hubs	No	No
Between-Network Variability Coefficient (BVC)	$BVC_n = \frac{1}{N'}\sum_{i'=1}^{n'}\sqrt{\frac{\sum_{l=1}^{T}(FC_{i'l} - \bar{x}_{FCl'})^2}{T-1}}$	Variable FC across tasks, between-network; flexible hubs	No	Yes
Network Flexibility (NF)	$Q = \frac{1}{2\mu}\sum_{ijlr}\{(FC_{ijl} - \gamma_l P_{ijl})\delta_{lr} + \delta_{ij}\omega_{jlr}\}\delta(Sil, Sjr)$ $NF_n = \frac{1}{N}\sum_{i=1}^{n}\frac{\sum_{ijlr}[Sij_{,lr} \neq Sij_{,l+1,r}]}{N(N-1)}$	Changes to community structure over time; malleable network affiliation	Yes	No
Network Partition Deviation (Deviation)	$Deviation_n = 1 - \left[\frac{\sum_{j=1}^{T}\left[\left(\max\left(\frac{\sum_{rS=1}^{c} FC_{cj}}{C}\right)\right) \in rS\right]}{T}\right]$	Network preference changes over time, compared to intrinsic partition; reassignment profile	Minimal	Yes

Table 1 summarizes the mathematical specifications of network metrics. Global variability coefficient (GVC; Cole et al. 2013b), between-network variability coefficient (BVC), network flexibility (NF; Bassett et al. 2011; 2013a; 2013b), and network partition deviation (novel) (named in ***column 1***) are described in terms of the following: (***Column 2***) their mathematical or algorithmic formulae. All equation symbols are expressed consistently. *Formula terms*: n=brain regions; T=tasks; i=region 1; l=task 1; N=number of regions; FC=adjacency matrix; n'=out-of-network regions; i'=region 1, out-of-network; N'=number of out-of-network regions; $FC_{i'l}$=edge weight, per out-of-network region, per task; FCl'=FC matrix, out-of-network regions only, per task; j=last region; r=last task; γ=spatial resolution; ω=temporal resolution; P=optimization null-model; $Sij_{,l+1,r=}S$, all other tasks; c=network regions; C=number of network regions; rS=predefined partition; FC_{cj}=edge weight, per network-region, per task; Q=multilayer modularity; δ=Kronecker's delta; S=network assignments. NF also lists the optimized quality function for community detection (Q-modularity, multilayer version, Mucha et al. 2010) because this was necessary before computing NF, and parameterization in the modularity algorithm was critical to our considerations. (***Column 3***) What each metric measured and diagnosed. This was how results were interpreted, and mechanisms or properties were framed. (***Column 4***) If each metric relied on user-chosen parameters (e.g., had a parameter-space). (***Column 5***) If each metric relied on a predefined network partition (also see Materials and Methods).

Materials and Methods

Participants

Right-handed, healthy adult participants (N=106) were recruited from Rutgers University and the surrounding Newark, New Jersey community. Six participants were excluded from analyses due to technical errors, leaving a total sample size of N=100 (see Extended Data Tables 1-1 and 1-2 for demographic characteristics). To improve replicability, we used a split-sample validation approach (Anderson and Magruder 2017) with a random subset of n=50 comprising a discovery dataset (Extended Data Table 1-1), and the remaining n=50 comprising a replication dataset (Extended Data Table 1-2). All participants provided informed consent in accordance with protocols approved by the Institutional Review Board of Rutgers University-Newark. Each participant provided or completed the following: (1) demographic information and intake survey questions, (2) the National Institutes of Health Cognition

Toolbox (Gershon et al. 2013), including a neuropsychological battery, (3) behavioral training on the C-PRO task (outside the scanner), (4) resting-state fMRI, and (5) C-PRO task fMRI. The subsets of data assessed herein included (1), (4), and (5) (see Schultz et al. 2019 for assessment of other variables). As listed in Extended Data Tables 1-1 and 1-2, there were no significant differences between identified genders on the distributions of age, ethnicity, or education.

Concrete Permuted Rule Operations (C-PRO) paradigm

The C-PRO paradigm was designed to involve rapid instructed task learning (RITL) through compositionally combining various task rules (Cole et al. 2010 & 2013a; Ito et al. 2017). We used a modified version of the PRO paradigm from Cole et al. (2010), which was previously introduced by Ito et al. (2017) (Fig. 1). This paradigm permutes four logic rules (both, not both, either, and neither), four sensory rules (red color, vertical orientation, high pitch sound, and constant tone), and four motor rules (left index, right index, left middle, and right middle fingers). This amounts to 12 rule sets represented 16 times across 64 unique task states. The software for presenting the task was E-Prime version 2.0.10.353 (Schneider et al. 2002).

In each task state, an initial instruction screen was presented for 3925 ms for participants to memorize a given permuted rule set (Fig. 1). This was followed by a jittered delay (1570 – 6280 ms, randomized from a uniform distribution), then three trials of paired audiovisual stimuli for participants to adjudicate based upon the given rule set (2355 ms each trial; inter-trial interval of 1570 ms). Another jittered delay occurred at the end of each task state (7850 – 12560 ms, randomized), which was immediately followed by the next permuted rule set instruction screen. An example instruction screen (Fig. 1; task state one) read: “BOTH, VERTICAL, LEFT INDEX”, indicating: “If both stimuli are vertical, press your left index finger”. In each of the three trials that followed, participants judged if both paired stimuli were vertically oriented, and either pressed the left index finger button to indicate “true” or the left middle finger button to indicate “false” (a judgement of “false” was always the same hand but opposite finger). Importantly, stimuli were always presented with auditory and visual features concurrently. Thus, focusing on the sensory rule given by the instructions was paramount (i.e., “VERTICAL” indicated that one should ignore auditory information, color information, and only focus on line orientation). Additionally, participants were required to remember and apply conditional logic and nontrivial motor commands each trial. Altogether this multitask behavioral paradigm is condition-rich and necessitates ongoing cognitive control.

Each participant completed a training session outside the scanner and a testing session within the scanner (task-state fMRI) 30 minutes later. During the training session participants equally practiced four rule sets that contained all 12 rules. This practice set was counterbalanced amongst participants and supplementary instruction was provided for training purposes (e.g., use the same hand but opposite finger to indicate “false”). Task fMRI scans were performed in eight runs, altogether containing 64 task state miniblocks, twice over (e.g., 128 task miniblocks), with each block composed of a permuted rule set (Fig. 1). Each task fMRI run was approximately eight minutes in duration, and identical miniblocks were never presented consecutively. Overall, mean performance was 83.47% correct (SD=9.00%). There was no significant difference in performance (percent correct) between males (M=83.65%, SD=10.44%) and females (M=83.33%, SD=7.80%); $t(74.71)=0.17$, $p=0.87$.

Study design and statistical analysis

Participants were randomly allocated to either a discovery dataset (n=50) or replication dataset (n=50). The replication dataset was not analyzed until after analyses of the discovery dataset were complete. Analyses of replication data were identical to analyses of discovery data (using the same code, including

all chosen parameters), and additionally included measures of similarity between replication and discovery results to quantify expected generalizability (Anderson and Magruder 2017).

The study progressed as follows (see following sections for details): (1) data collection and separation into discovery and replication sets, (2) fMRI pre-processing and regional parcellation, (3) functional connectivity estimation, (4) network metric calculations, (5) application of the network partition (metric typically averaged across regions within each network), (6) statistical analyses, (7) creation of cognitive control cartographies, and (8) replication analyses (i.e., repeat steps 2–8 for replication dataset). Whenever multiple comparisons were addressed, we utilized nonparametric permutation testing with maxima-derived 95% confidence intervals for statistical hypothesis testing against zero (Blair and Karniski 1993; Nichols and Holmes 2002). This resampling approach is powerfully suited for variables that have no assumed distribution, and it provides exact statistics that are data-driven. Henceforth we will describe maxima-derived statistics as max-T. We used the Rutgers University high-performance computing cluster (https://oarc.rutgers.edu) when necessary, and performed 10,000 permutations per test (unless otherwise specified in the Results). To analyze the similarity of two correlation (adjacency) matrices we used the Mantel permutation test, which performs a Pearson's correlation across the upper triangles (off-diagonal) of the adjacency matrices (Mantel 1967; Glerean et al. 2016). The Mantel test is more conservative than a standard comparison between connectivity matrices because it takes into account the fact that observations in distance/similarity matrices are not independent (an assumption of both parametric and standard non-parametric tests). In each Mantel analysis, we again used nonparametric permutation procedures to derive statistics that make minimal assumptions about probability distribution (10,000 permutations unless otherwise specified). Henceforth we will describe these matrix similarity statistics as Mantel-r.

MRI parameters

All MRI data were collected at the Rutgers University Brain Imaging Center (RUBIC). When possible, the best practices suggested by the Human Connectome Project preprocessing pipelines were followed (Glasser et al. 2013). A 3T, 32-channel head coil within a Siemens Trio scanner was used to obtain multiband, whole-brain, and echo-planar imaging (EPI). The repetition time (TR) was 785 ms; the echo time (TE) was 34.8 ms; the flip angle was 55°; the bandwidth was 1924 Hz/Px; the in-plane field-of-view (FoV) read was 208 mm; 72 slices; 2.0 mm isotropic voxels; and the multiband acceleration factor was 8. Whole-brain and high-resolution T1-weighted and T2-weighted anatomical scans were also acquired, with an isotropic voxel resolution of 0.8 mm. Spin echo field maps were obtained in both the anterior-posterior and posterior-anterior directions. Resting-state fMRI scans were 14 minutes in duration, amounting to 1070 TRs. Each task (i.e., C-PRO) fMRI run was approximately eight minutes in duration, adding up to approximately one hour in the scanner for the task session (36 TRs per task miniblock; 4608 TRs altogether).

fMRI preprocessing

The open-source Human Connectome Project minimal preprocessing pipeline (Glasser et al. 2013), version 3.5.0, was applied to all neuroimaging data. This included: anatomical reconstruction and segmentation; EPI reconstruction, segmentation, and spatial normalization to a standard template; intensity normalization; and motion correction. The resulting data was in CIFTI 64k-vertex grayordinate space, and all subsequent analyses were performed in MATLAB R2014b (The Mathworks, Inc.). Following minimal preprocessing, vertices were parcellated into 360 cortical regions (180 per hemisphere) per the Glasser et al. (2016) atlas. This parcellation scheme was previously developed with a large sample size

dataset containing multimodal images that yielded high inter-subject alignment (Glasser et al. 2016). To parcellate each of these regions, we calculated the average time series of enclosed vertices.

Next, we performed nuisance regression on parcellated resting-state and task-state data using 6 motion parameters plus their derivatives (totaling 12 motion parameters), and volumetrically-extracted ventricle and white matter timeseries (via FreeSurfer http://surfer.nmr.mgh.harvard.edu/), plus their first derivatives (16 regressors overall). Note that global signal was not removed due to evidence that it can artificially introduce negative relationships (Murphy et al. 2009). Task time series were further processed to account for event-related activity by fitting a general linear model (GLM) to task activity estimated by a finite impulse response (FIR) function. FIR modeling uses flexible basis sets and event-based design matrices that have been shown to provide more accurate and stable estimates than a canonical hemodynamic response function (Fair et al. 2007; Cole et al. 2019).

Functional connectivity estimation

Functional connectivity (FC) was estimated for parcellated (region-wise) data, per participant and per state. Across the whole cortex, we utilized Pearson correlation coefficients to compute interregional relationships of blood-oxygen-level dependent (BOLD) timeseries, resulting in 360 by 360 connectivity matrices. Given the complex nature of subsequent analyses (i.e., network metrics) we chose this method of FC estimation for simplicity and wide-reaching comprehension. However, probing other methods of FC estimation is warranted in future studies (Zalesky et al. 2012; Cole et al. 2016). To implement Pearson's correlation, we used MATLAB's *corrcoef* function, which employs the following formula:

$$R(A,B) = \frac{1}{N-1}\sum_{i=1}^{N} \left(\frac{A_i - \mu_A}{\sigma_A}\right)\left(\frac{B_i - \mu_B}{\sigma_B}\right)$$

In this formula, μ refers to the mean and σ refers to the variance. This was applied to all pairwise combinations of N regions (360) and resulted in square adjacency matrices of interregional correlation coefficients. Following this, all arithmetic or statistical procedures (e.g., averaging) were performed with the Fisher Z-transformation to stabilize variance.

Network metrics

Interregional connectivity was probed by three network metrics for state-based reconfiguration properties (Medaglia et al. 2015): (1) Global variability coefficient (GVC; Cole et al. 2013b, and relatedly, between-network variability coefficient (BVC; novel but related to Ito et al. 2017), (2) Network flexibility (NF; Bassett et al. 2011 & 2013a), and (3) Network partition deviation (deviation; novel). Figure 2 illustrates the algorithms of these metrics schematically. Table 1 summarizes the primary characteristics of these metrics, including formulae, interpretations, parameter-space considerations, and reliance on a predefined network partition. A predefined network partition is sometimes called a "hard partition", and refers to the use of a predefined network or community assignment structure, such that each parcellated region is indexed into the partition *a priori* (Sporns and Betzel 2016).

Global Variability Coefficient (GVC)

GVC was originally developed by Cole et al., (2013b), and characterizes changing patterns of connectivity across task states by measuring the variability of interregional connectivity (Fig. 2A). Thus, GVC treats spatial changes in connectivity, across states, as continuous. This results in a unitary estimate across time (i.e., one standard deviation per region, across time or task states), which we describe as a semi-

discretized treatment of temporal changes in connectivity. No parameters are required by the user and a predefined network partition is not necessary (aside from regional parcellation, as in the present study) (see Table 1).

In Cole et al., (2013b), FPN connectivity was found to vary systematically with similarity of C-PRO task states, demonstrating that GVC results were not driven by noise. We replicated this finding and extended the analysis to CON connections. In brief, the 64 C-PRO task states have zero to two overlapping rules (Fig. 1). For example, one task's rules included *both, high pitch,* and *left middle*, and another included *both, red,* and *left middle*. These example tasks had two overlapping rules (*both* and *left middle*). We created a 64 by 64 similarity matrix to quantify these overlap sets, and quantified the Spearman's Rho for FPN and CON connections for those sets. Next, we restricted the same analysis by only including FPN and CON regions with the highest GVC, in the following increments: top 10%, 8%, 6%, 4%, and 2%. This addresses whether highly variable connectivity (as measured by GVC) relates systematically to task context (Cole et al. 2013b).

Between-Network Variability Coefficient (BVC)

BVC was inspired by Cole et al. (2013b), and is related to between-network global connectivity (BGC) in Ito et al. (2017). BVC is equivalent to GVC, except within-network connectivity estimates are withheld from the computation of standard deviation (Fig. 2A). Thus, BVC (unlike GVC) required the use of a predefined network partition to define the regional bounds of each network. Additionally, spatial changes were treated as semi-continuous given that internetwork estimates were ignored. All other specifications of BVC are identical to GVC (see Table 1).

Network Flexibility (NF)

NF was originally developed by Bassett et al. (2011; 2013a; 2013b), and characterizes the spatiotemporal dynamics related to task-state time series by quantifying temporal variability in network partition solutions (see Table 1 and Fig. 2B). These network partitions are determined by an optimized quality function termed multilayer modularity (also termed multislice or multiplex in some studies) (Mucha et al. 2010). Thus, NF does not utilize a predefined network partition, but instead requires community detection to be applied per dataset. Required parameters (γ,ω) could be used to tune the degree to which connections were treated as discrete versus continuous in space (γ is the spatial resolution parameter) and/or time (ω is the temporal resolution, or coupling, parameter). In the present study, we swept a parameter space of γ and ω, ranged around their prototypical values (Chen et al. 2015). Given the standard use of γ=1 (Bassett et al. 2013a; Braun et al. 2015), spatial reconfigurations were treated as discrete, or solitary, by NF. The temporal parameter, ω, is typically set to a value of 1.0 in the multilayer version of the community detection algorithm (Bassett et al. 2013a; Braun et al. 2015; Amelio and Tagarelli 2017). NF is therefore coupled, or driving, in the temporal dimension. Thus, we considered NF to treat changes in connectivity (vis-à-vis community structure changes) across time as dynamic. We swept the modularity function's parameter space by ranging ω from zero to 2.0 in steps of 0.2; and γ from zero to 5.0 in steps of 0.5. For both free parameters, zero is the lower limit. An upper limit of 2.0 for ω was based on prior observations that task states tend to merge into one large state at higher coupling values (Bassett et al. 2013a). At the upper limit of γ (5.0), spatial resolution becomes acute and each region develops its own network. Additionally, the temporal dynamics conferred by ω are no longer available at the upper limit of γ (Chen et al. 2015; Amelio and Tagarelli 2017). This sweep yielded an 11 by 11 matrix of NF estimates, per region (and per participant). We later compared regional NF estimates to regional GVC estimates (both metrics were standardized, and Spearman's rank-order correlation quantified similarity in these measures across participants), to assess the point in the parameter-space

wherein NF and GVC overlap most. These comparisons were performed for both the network-mean and regional-mean vectors. The results section depicts NF estimates for (1) the field-standard point in this parameter space (termed "NF-standard"; γ=1 and ω=1), (2) the point of highest similarity between NF and GVC (termed "NF-matched"; γ=2.5 and ω=0.2), and (3) the point of lowest similarity between NF and GVC (termed "NF-unmatched"; γ=0.5 and ω=0.2). In the case of NF-unmatched, the network-wise comparison with GVC maintained two points in the parameter space with equivalently low Spearman's Rho estimates (the other point was yielded by γ=4.5 and ω=0.2). The combination of γ=0.5 and ω=0.2 was chosen because it also generated the lowest Rho in the region-wise comparison.

Network Partition Deviation

To reconcile divergent principles and results of GVC and NF (see Results), we created a novel metric termed network partition deviation (or just "deviation"). The primary goal of developing deviation was to quantify network reconfiguration in a highly principled manner. This involved a principled definition for what it means for a region to "reconfigure": a change in the network community that a given region is most connected with (i.e., network with the highest mean connectivity). Deviation enumerated network reassignments from a predefined partition across task states (see Table 1 and Fig. 2C). Per task state and per region, the maximum connectivity estimate was found and its location relative to the predefined partition was indexed as the "preference" for that given state. That is to say, each region's connectivity estimates (across the other 359 regions) were searched for the maximum connectivity value, per task state. Then, the network this value belonged to was indexed as the preferred network assignment for that state. To illustrate how network reassignment was computed, we generated a video of the regional network preferences across task states, projected onto a standard brain schematic (see Multimedia 1). We used the Human Connectome Project's Workbench software to generate these visualizations (Marcus et al. 2011).

Deviation was the percent of task states (more generally, the relative frequency across time), in which a given region's preference *deviated* from the predefined partition. We used the Cole-Anticevic brain-wide network partition (Ji et al. 2019), plus adjustments derived from the empirical resting-state fMRI data of the participants studied herein, as the predefined reference (see below for more details on network partitioning). Deviation may be accompanied by its complementary measure, network partition adherence, which was the relative frequency of states in which a given region *adhered* to its predefined network assignment (or 1-deviation, meaning that deviation and adherence add up to 1, or 100% of task states).

We further unpacked deviation by depicting *which* networks were preferred by regions (when deviating from the partition), and generated reassignment profiles. An *a priori* network partition was required by deviation insofar as it was based upon a predefined reference. This reference acted as a parameter in the algorithm given that it delineates predefined values that impact the deviation score. However, it acted within a conditional-logic operation ('is an element of' from set-theory; see Table 1), not a transformative operation (such as a constant value used for multiplication, e.g., γ). We thus considered deviation to only minimally maintain a parameter-space in Table 1, particularly given the option for researchers to apply a community detection algorithm to their empirical data if they see fit. Altogether, deviation is a principled approach that is poised to address a variety of problems related to network reconfigurations between states.

Network partition

We applied the cortical portion of the Cole-Anticevic brain-wide network partition (CAB-NP) (Ji et al. 2019; Fig. 3D and Extended Data Fig. 3-1), which was based on publicly available Human Connectome

Project data. The CAB-NP was based on resting-state fMRI data across the whole brain, and used the Louvain community detection algorithm to assign parcellated cortical regions (Glasser et al. 2016) into 12 functional networks. The CAB-NP corroborated features of well-known cortical partitions (Gordon et al. 2016; Power et al. 2011; Yeo et al. 2011), yet found novel but robust networks.

We first partitioned resting-state data by sorting regional FC estimates per the 12 CAB-NP network indices. We then found the maximum FC estimate (i.e., the intrinsic "preference") for each region (per participant), and tested if its location was equivalent to the CAB-NP. If this index was different from the CAB-NP in over 50% of participants, we reassigned that region to its empirically-derived preference. We henceforth used this empirically-adjusted CAB-NP to sort task-state data into networks (see Extended Data Fig. 3-1). Network metrics were computed across states and averaged across regions that compose a given network, per participant. In analyses that used standardized metrics (i.e., z-scores), standardizations were performed before network averages and standard errors were computed.

In select analyses, we probed the similarity of two partitions. To accomplish this, we used the Jaccard index, which is a standard measure of similarity from set theory. For example, the Jaccard index was used to assess the similarity of the empirically-adjusted resting-state partitions of the discovery and replication datasets. We used the MATLAB *jaccard* function, which utilized the "intersection over union" formula on label vectors A and B, with the following equation:

$$jaccard(A,B) = |intersection(A,B)|/|union(A,B)|$$

Per state, the intersection equaled the number of true positives (i.e., overlap of two partitions), and the union was the number of true positives summed with the number of false positives and false negatives.

Cognitive control cartographies

We rendered one primary mapping of cross-state network-reconfiguration properties, and two secondary mappings which broke up the primary mapping's properties into within-network and between-network scores. In the primary cartography, network-mean scores on GVC and deviation were plotted together to chart global and local properties, respectively. Each of these metrics were computed exactly as described above. In the two secondary cartographies, GVC and deviation were expanded by their within-network and between-network scores.

Within-network GVC was computed by setting between-network FC estimates to 'NaN' (i.e., 'not a number' in MATLAB) before inputting data into the GVC algorithm. Likewise, between-network GVC was computed by setting within-network FC estimates to 'NaN'. This effectively nullified the variability for those regions such that GVC ignored them during computation (which principally employs standard deviation across states; see Fig. 2A and Table 1). Between-network GVC was equivalent to BVC described above. Within-network deviation was computed by setting FC estimates of between-network regions to the resting-state FC for those regions before inputting data into the deviation algorithm. Likewise, for between-network deviation, we substituted within-network estimates with corresponding regions' resting-state FC. We considered the use of resting-state FC most appropriate given deviation's inherent comparison to the resting-state partition. That is to say, deviation away from the resting-state partition would always be zero for regions set to their resting-state estimates. Extended Data Fig. 7-2 visually depicts the input data schemes for each of these secondary cartographies.

All networks were mapped according to these specifications, with special focus on cognitive control networks (highlighted in Fig. 7). We further tested if the four measures employed in the cartographies were significantly different according to control network grouping (across participants)

using a multivariate analysis of variance (MANOVA). To accomplish this, we used the MATLAB *manova* function.

Code & Software Accessibility

We included all MATLAB, python, and demo code in a publically available platform. Data is available at the level of functional connectivity estimation, for the use of loading into demo scripts. Data at other levels of processing, or data otherwise presented in this study, are available upon request. The master GitHub repository for this study can be found here: https://github.com/ColeLab/controlCartography

Results

Intrinsic and Task-State Functional Connectivity

Replicating previous findings (Cole et al. 2014), cortex-wide rsFC (Fig. 3A) and tFC (Fig. 3B) estimates were highly similar. This significant similarity was observed for the average tFC taken across all 64 C-PRO tasks (r=0.89, p<0.00001, R^2=0.79), as well as for each C-PRO rule individually (Extended Data Table 3-1). This aligns with previous observations that the set of resting state networks is highly related to the set of networks present during task states. In addition to the minimal cognitive demands during rest providing a cognitive baseline for a variety of tasks, this result suggests that rest may be an appropriate reference state for characterizing changes in networks across multiple task states. The similarity observed between rsFC and tFC (all 64 C-PRO tasks) in the *replication* dataset was comparable (r=0.90, p<0.00001, R^2=0.81).

To summarize changing connectivity from the resting state to the average task state, we firstly assessed each state (rest and task) individually. Approximately 95% of resting-state connections (Fig. 3A) were significantly different from zero, based on a randomly permuted null model (max-T correction for multiple comparisons, critical threshold=6.07, 5,000 permutations). Approximately 79% of task-state connections (Fig. 3B) were significantly different from zero, again based on a randomly permuted null model (max-T critical threshold=5.92, 5,000 permutations). Next, we created a task versus rest difference matrix (Fig. 3C), and found 21% of those values to be significant differences (max-T critical threshold=5.46, 5,000 permutations). Of the significant rest-to-task changes, approximately 99% were decreases in connectivity; 1%, increases. The tendency for connectivity to decrease from the resting-state to task states is consistent with prior observations of this same phenomenon in both fMRI and multi-unit spiking data (Ito et al. 2019). Moreover, the finding that rsFC and tFC (across multiple task states) are highly correlated, yet the differences between them are nontrivial, justified subsequent analyses of functional reconfigurations between these two kinds of states.

Findings were consistent in the *replication* dataset (5,000 permutations in each test): approximately 95% significant resting-state connections (max-T critical=6.06); approximately 74% significant task-state connections (max-T critical=5.92); and approximately 32% significant rest-to-task differences (max-T critical=5.67). Likewise, 100% of the rest-to-task changes were decreases in connectivity in the replication dataset.

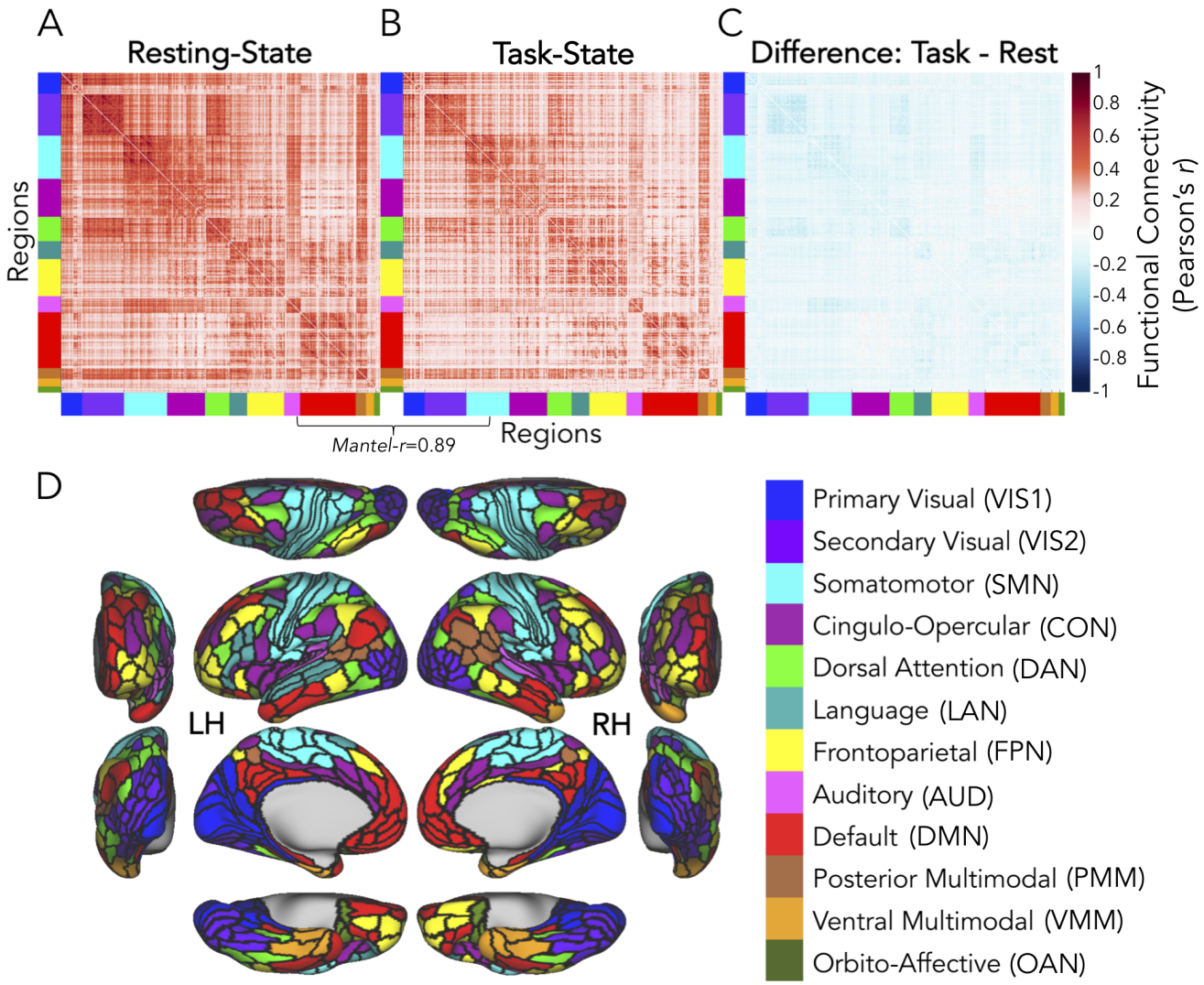

Figure 3. Functional connectivity (FC) estimation. (***A***) Resting-state functional connectivity (rsFC) across 360 by 360 regions (regional parcellation as in Glasser et al. 2016), ordered per the CAB-NP, adjusted by resting-state preferences (see Materials and Methods) (color-coded along each matrix edge as in D). Values are discovery-set grand averages. (***B***) Task-state functional connectivity (tFC) across 360 by 360 brain regions, ordered and estimated as in A (grand averages: n=50 and 64 C-PRO task states). (***C***) Difference matrix: [tFC – rsFC]. (***D***) Cortical schematic of the Cole-Anticevic Brain-wide Network Partition (CAB-NP) (Ji et al. 2019), empirically adjusted by the resting-state preferences of the present participants (see Materials and Methods). LH = left hemisphere; RH = right hemisphere. Color-coding scheme of networks and acronyms listed in parentheses are used consistently throughout the present paper. Note that the two cognitive control networks of special interest included the CON (plum) and FPN (yellow).

Network Metrics: Variability Coefficients

Our prior work found that the FPN contains *flexible hub regions* – network nodes capable of rapid reconfiguration with changing task demands (flexible) that have extensive connectivity (hubs) (Cole et al. 2013b). Recent work has suggested that the CON also contains hub-like regions (Ito et al. 2017; Power et al. 2013), yet it is unknown if they are likewise flexible. Accordingly, we used two related metrics to assess if networks contain flexible hub regions (Cole et al. 2013b): global variability coefficient (GVC), and between-network variability coefficient (BVC) (see Materials and Methods, Fig. 2, and Table 1).

GVC was originally developed by Cole et al. (2013b), and quantifies the average variability in global connectivity across task states (Fig. 2A and Table 1). In that study, the frontoparietal network

(FPN) exhibited the highest GVC compared to all other networks. The FPN also demonstrated that connectivity patterns could decode task information (using an earlier version of the C-PRO paradigm). Systematic changes to the global FPN connectivity patterns enabled this decodability; a property that was termed *compositional coding*. Taken together, the FPN was reported to contain regions exerting adaptive task control as flexible hubs.

BVC is equivalent to GVC, but excludes within-network connections (Fig. 2A and Table 1). This change from GVC accounts for the potential confound that within-network connections might confer upon results. A related measure, BGC (between-network global connectivity), was introduced by (Ito et al. 2017) to identify networks containing hub-like regions during rest. Herein, BVC was additionally inspired by findings in Cole et al. (2013b), which suggested flexible hubs in the FPN were not driven by within-network connections. In that study, FPN had the highest participation coefficient compared to all other networks. This suggests that FPN regions maintain
many between-network connector hubs; BVC simply quantifies this in a manner closer to GVC.

Critically, Cole et al. (2013b) only involved N=15 subjects, compared to the N=50 *discovery* and separate N=50 *replication* datasets in the present study. Thus, replicating the results of Cole et al. (2013b) would be nontrivial. Replicating the main result of Cole et al. (2013b), regions of the FPN had the highest GVC (Fig. 4A) and BVC (Extended Data Fig. 4-2A and 4-2B) compared to the mean of all other networks (GVC: max-T(49)=10.94, $p<0.0001$; BVC: max-T(49)=10.69, $p<0.0001$). BVC and GVC results were highly correlated at both the network (Fig. 4A) and regional levels (Fig. 4B) (network-wise: r=0.9912, $p<0.00001$, $R^2=0.9824$ cross-network shared variance; region-wise: r=0.9972, $p<0.0001$, $R^2=0.9944$ cross-region shared variance), suggesting that within-network estimates do not dominate the outcome of GVC analyses (see Extended Data Fig. 4-3A and 4-3B).

These results replicated in the *replication* dataset: the FPN demonstrated the highest GVC (Extended Data Fig. 4-1) and BVC (Extended Data Fig. 4-2C and 4-2D) compared to the mean of all other networks (GVC: max-T(49)=7.23, $p<0.0001$; BVC: max-T(49)=6.93, $p<0.0001$). BVC and GVC results were also tightly correlated at both the network and regional levels in the *replication* dataset (network-wise: r=0.9925, $p<0.00001$, $R^2=0.985$ cross-network shared variance; region-wise: r=0.9975, $p<0.0001$, $R^2=0.995$ cross-region shared variance) (Extended Data Fig. 4-3C and 4-3D). Additionally, both GVC and BVC results highly overlapped between discovery and replication datasets (GVC: *Rho*=0.9091, $p<0.00001$; BVC: *Rho*=0.881, $p=0.0002$) (Extended Data Fig. 4-1 and 4-2).

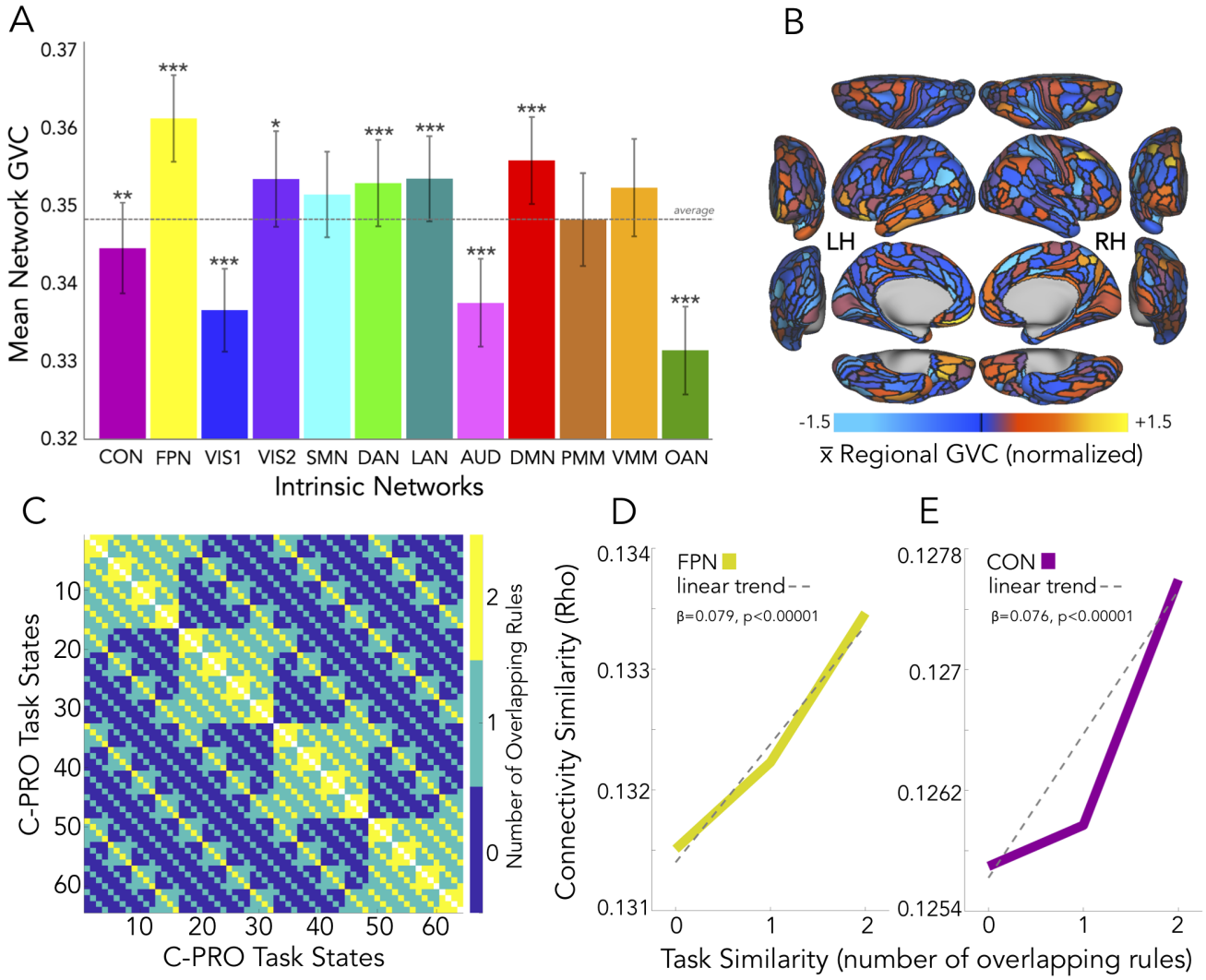

Figure 4. Global variability coefficient (GVC). (***A***) Network-mean GVC. Means were across n=50 and all C-PRO task states; error bars represent standard error of the mean. Asterisks mark statistically significant t-tests, using the max-T approach (see Materials and Methods; 10,000 permutations). The grey dashed line represents the mean GVC value across networks. (***B***) Regional-mean GVC. (***C***) The similarity of C-PRO task states, represented by number of overlapping rules (0 overlapping rule=blue, 1 overlapping rule=green, 2 overlapping rules=yellow). Note that an overlap of 3 rules exists along the diagonal (white boxes), but these connections were not included in analyses because they represent identical task states, wherein connectivity similarity would necessarily be *Rho*=1. (*D*) The relationship between connectivity similarity (as measured by Spearman's Rho) and task similarity. FPN is depicted in yellow. All connectivity estimates were included (i.e., no thresholding). The linear trend is depicted by a dashed gray line, with the associated beta coefficient and t-test significance listed. (***E***) Same as C, but for CON regions (depicted in plum). The results in D and E demonstrated that connectivity of control network regions varied systematically with task similarity, suggesting that GVC results (A and B) were not driven by network noise.

In conjunction with many studies reporting increased FPN activity as a function of cognitive control demands (Yeo et al. 2015), this pattern of results supports the notion that the FPN contains flexible regions adaptively configured for multitask control. Further, we compared GVC between control networks and all other networks. FPN regions were significantly higher than each other network (using the max-T approach, $p<0.0001$), except for the ventral multimodal network (orange bar in Fig. 4A). CON regions were significantly different (typically lower) than each other network on the measure of GVC (using the max-T approach, $p<0.0001$), except for posterior multimodal and ventral multimodal networks

(brown and orange bars in Fig. 4A, respectively). Lastly, a paired-samples t-test comparing FPN and CON revealed a significant difference in GVC scores ($t(49)=11.68$, $p<0.00001$), suggesting that the two proposed control networks exhibit distinct variability of global connectivity. In the *replication* dataset, FPN regions' GVC scores were also significantly higher than each other network, except for the ventral multimodal network (orange bar in Extended Data Fig. 4-1). CON regions were significantly different than each other network on the measure of GVC in the *replication* dataset, with no exceptions (Extended Data Fig. 4-1). The paired-samples t-test contrasting FPN and CON specifically also showed a significant difference on GVC scores in the *replication* dataset ($t(49)=10.55$, $p<0.00001$).

Despite evidence that FPN has strong global variability consistent with flexible hubs, it remains unclear if that variability is systematically related to task information content – a prerequisite for flexible hubs to implement task-related reconfigurations. Prior findings (Cole et al. 2013b) demonstrated that FPN connections systematically vary with increasing task-state similarity (Fig. 4C-4E). We sought to replicate this result in FPN and – given the current focus on cognitive control systems – we additionally analyzed CON connections. As in Cole et al. 2013b, task-state similarity was taken as the number of overlapping, or shared, rules presented to participants, across all 64 tasks (Fig. 4C; also see Materials and Methods). We then measured Spearman rank correlations (as a score of similarity) amongst connections according to these task-state pairings, for both FPN (Fig. 4D) and CON regions (Fig. 4E). An approximately linear relationship was observed, suggesting that shifts in connectivity systematically relate to shifts in task state, and are not simply a byproduct of noise. The linear regression weights of these similarity scores were statistically different from zero, across subjects (FPN: $t(49)=35.51$, $p<0.00001$; CON: $t(49)=33.25$, $p<0.00001$). Next, we performed the same analyses, but restricted the connections to those maintaining the highest variability (across top 2% to 10% in steps of 2%) across task states (i.e., the "VC" of GVC) for both the FPN (as in Cole et al. 2013b) and CON. Results were similar to the main results across all thresholds, with linear weights significantly different from zero ($p<0.05$). These results suggest that GVC results are likewise driven by systematic changes in connectivity, and not network noise. These results additionally reveal that CON also systematically changes its global connectivity pattern according to task goals, though the GVC results suggest these systematic changes are smaller in CON than FPN (and most other networks).

Network Metric: Flexibility

Network Flexibility (NF) (Fig. 2B) measures functional network dynamics related to task-state time series (Bassett et al. 2011; 2013a; 2013b), and is thus highly relevant to our current hypotheses regarding control network reconfigurations. Conceptually, NF is aligned with GVC, particularly as both quantify large-scale changes in functional network configurations. However, it is unknown whether these metrics capture the same aspects of network reconfiguration. The equations and specifications listed in Table 1 predict that while both are oriented around a measure of network change, the approaches are distinct enough to hypothesize that NF and GVC will not entirely overlap. We hypothesized that differentiation between NF and GVC would lend insight into the nature of control network reconfiguration. In particular, GVC assesses continuous changes in connectivity strengths, while NF assesses discrete network reassignments.

We used the previously-developed "categorical" version of NF (Cole et al. 2014). Briefly, this involved first identifying network assignments for each task state, irrespective of the resting-state partition. These assignments were yielded by passing tFC estimates through a multilayer quality function for community detection (Louvain Q-modularity; Mucha et al. 2010). Next, regional assignments were assessed for how well they were maintained across task states, which is termed "modular allegiance"

(Bassett et al. 2011). NF quantifies how often (i.e., for how many tasks) a region changed its allegiance, and standardizes this by all possible changes (see Materials and Methods, Fig. 2B, and Table 1).

The multilayer modularity step required parameters ω (temporal resolution or "coupling") and γ (spatial resolution) to be chosen. The standard values used for these parameters across multiple studies are γ=1 and ω=1 (Bassett et al. 2013b; Chen et al. 2015; Braun et al. 2015). NF that resulted from community detection at γ=1 and ω=1 was termed "NF-standard" (Fig. 5C). Since there is only limited theoretical basis for those parameter choices we computed NF across a range of values around these standards, such that γ was varied between zero and five in steps of 0.5; and ω was varied between zero and two in steps of 0.2 (see Materials and Methods). These sweeps resulted in 121 vectors of regional NF estimates (per participant). We compared resulting NF values to GVC values (Fig. 5A & 5B), and found that NF was most strongly correlated with GVC when γ=2.5 and ω=0.2 (Rho=0.8169, $p<0.00001$); we termed this "NF-matched" (darkest red boxes in Fig. 5A & 5B; scatter plot in Fig. 5D). In the regional *replication* analyses, "NF-matched" was found at γ=3 and ω=0.2 (see Extended Data Fig. 5-1), demonstrating a similar spatial resolution (γ=2.5 versus γ=3) for the highest correlation between NF and GVC in the replication dataset. However, at the network level, γ=2.5 and ω=0.2 yielded the highest correlation between NF and GVC in the replication dataset (corresponding to the discovery dataset). NF-standard was not significantly correlated with GVC (Rho=0.4546, $p=0.14$) (Fig. 5C). Lastly, we probed the free-parameter combination that yielded flexibility scores least correlated with GVC, termed "NF-unmatched", which occurred at γ=0.5 and ω=0.2 (Rho=-0.4546, $p=0.14$) (darkest blue boxes in Fig. 5A & 5B; scatter plot in Fig. 5E). Similar to NF-matched, NF-unmatched was likewise yielded by the same parameter combination (γ=0.5 and ω=0.2) at the network level in the replication dataset (see Extended Data Fig. 5-1). Moreover, FPN regions exhibited significantly higher NF-matched values relative to the mean of all other networks (max-T(49)=4.42, $p<0.0001$) (Extended Data Fig. 5-2). In the replication dataset (using the parameters identified in the discovery dataset to avoid circularity), FPN regions were significantly higher on NF-matched compared to the mean of all other networks as well (max-T(49)=3.60, $p<0.0001$). NF estimates overlapped between discovery and replication datasets (NF-matched *Rho*=0.713, $p=0.012$; NF-standard *Rho*=0.930, $p<0.00001$; NF-unmatched *Rho*=0.902, $p<0.00001$).

We propose that NF-matched captured a near-continuous distribution of connectivity values via higher spatial resolution (γ) (creating many small networks), which was offset by a moderate temporal resolution (ω) that kept all the states from merging into one large state (see Extended Data Fig. 5-3 for community assignment structure). The comparatively high NF-matched maintained by the FPN suggests that in this sector of the parameter space, the FPN flexibly reorganized across task states more than other networks. NF-standard, however, resulted in an undersized number of networks due to the lower spatial resolution, masking some of the dynamics that were available to GVC (which did not merge connections into networks prior to computing connectivity dynamics). These results help reveal the relationship between two dynamic connectivity measures in the literature (GVC and NF), which we build on in the following section.

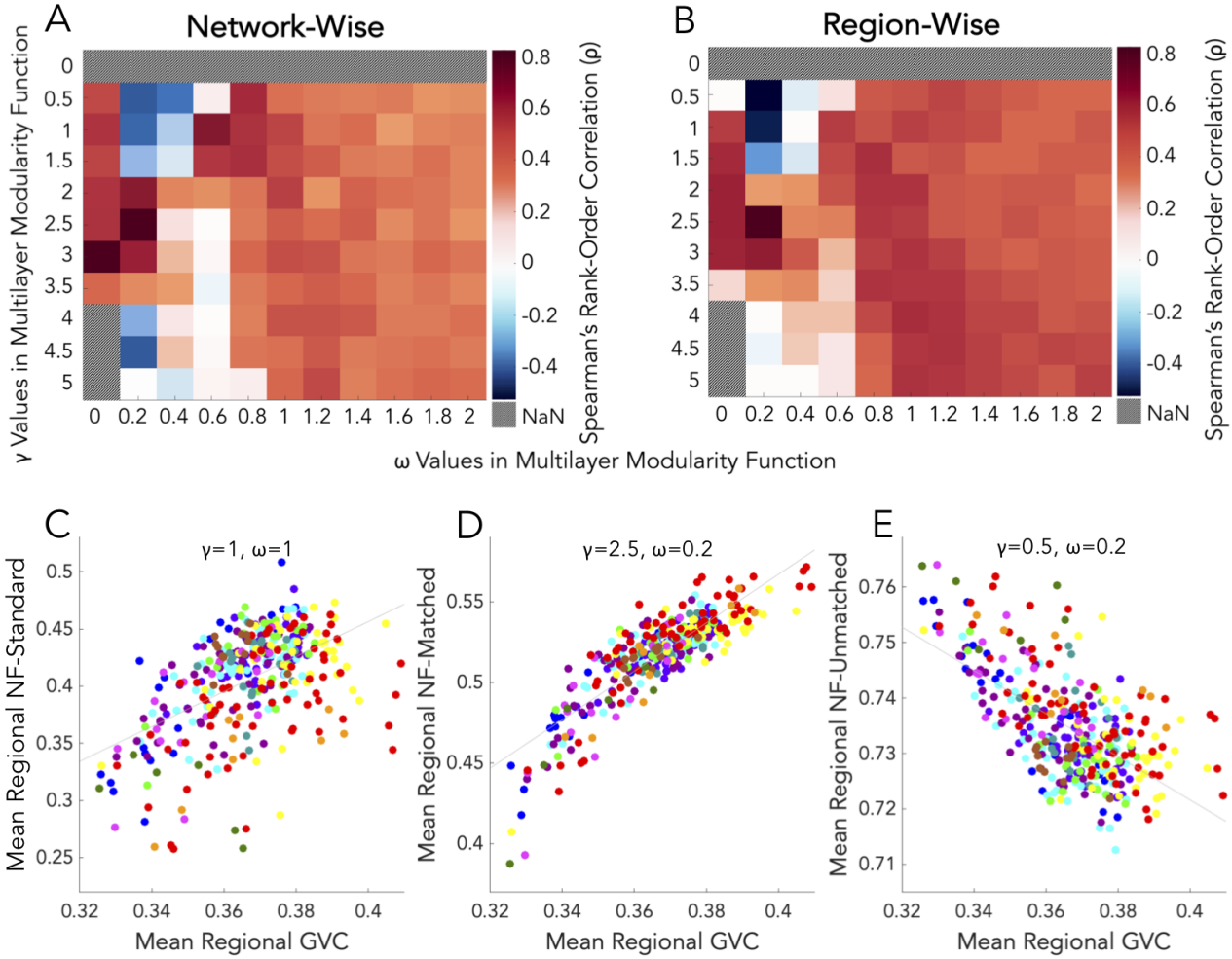

Figure 5. Comparison of global variability coefficient (GVC) and network flexibility (NF). (***A***) Network-wise comparisons (Spearman's rank order correlation) of GVC and NF sweeped by multilayer modularity parameters, across participants. (***B***) Same as A, but at the region-wise level. (***C***) Regional mean GVC plotted over regional mean NF-standard (multilayer modularity parameters: γ=1 and ω=1). NF-standard results were yielded by the standard parameter combination. Each region (mean across N=50 participants) was plotted as individual scatter points, and color-coded according to the network it belongs to (as in Fig. 3D). (***D***) Same as C, but with NF-matched represented on the y-axis (γ=2.5 and ω=0.2). This parameter combination yielded NF results most correlated with GVC (or, "matched"), as depicted in A and B by dark red squares. (***E***) Same as C and D, but with NF-unmatched represented on the y-axis (γ=0.5 and ω=0.2). This parameter combination yielded NF results least correlated with GVC (or, "unmatched"), as depicted in A and B by blue squares. The inconsistency of this result with the results in panels C-E suggested the need for a new measure of network switching that was less dependent on parameter selection.

Network Metric: Partition Deviation

Given that GVC and NF demonstrated inconsistent results dependent on tuning parameters, we created a novel metric, Network Partition Deviation, to reconcile the principles underlying these metrics. Specifically, we sought a principled definition of network reconfiguration that would reflect the goals of NF, without the need for a parameter search. Deviation enumerates network reassignments across task states by quantifying the percent of states (i.e., the relative frequency across tasks) in which a given region deviates from a predefined partition (see Materials and Methods, Fig. 2C, Table 1, and Multimedia 1). We employed the CAB-NP adjusted by the empirical resting-state data of participants herein (Fig. 3D) as the intrinsic, predefined reference. See prior work (Cole et al. 2014; Krienen et al. 2014) and the results

section "Intrinsic and Task-State Connectivity" above for evidence that the resting state provides an appropriate intrinsic network configuration to act as a reference for assessing network deviations.

Of the proposed cognitive control networks – the CON and the FPN – the CON displayed the highest mean deviation, which was significantly higher than the mean across all other networks (max-T(49)=12.74, $p<0.0001$) (Fig. 6A). Moreover, the FPN demonstrated deviation that was near the mean, and was not significantly different from the mean across all other networks. This contrasted from the conclusions drawn from GVC and NF, which showed the FPN significantly above the mean, and the CON significantly below it. Similarly in the *replication* dataset, CON regions' deviation scores were again significantly higher than the mean of all other networks (max-T(49)=16.33, $p<0.0001$) (Extended Data Fig. 6-1A).

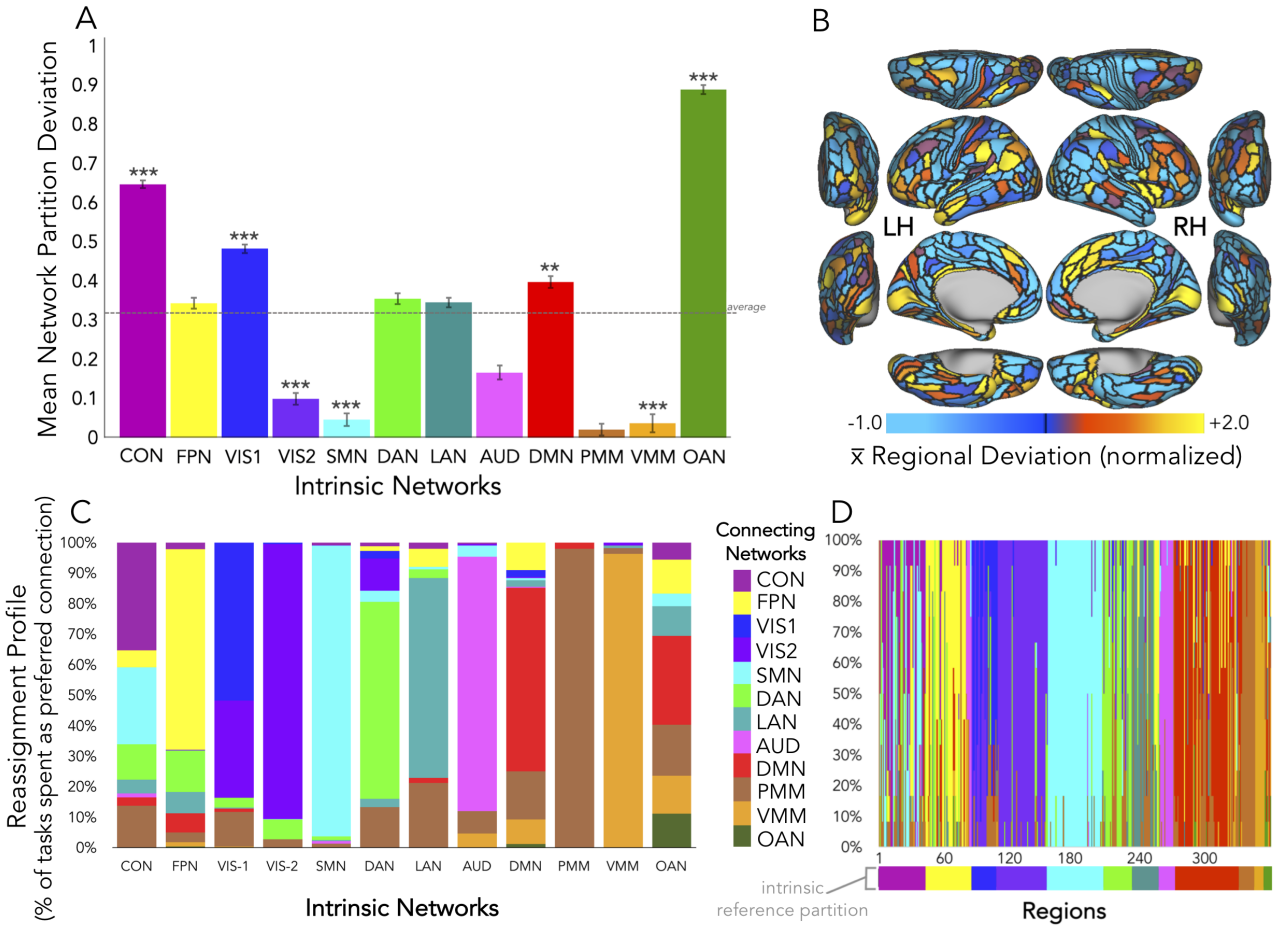

Figure 6. Network Partition Deviation. Mean, error bars, and hypothesis testing specifications were the same is in Figs. 5 & 6. (***A***) Network-mean deviation. See Discussion section for interpretations of the orbito-affective network (OAN). (***B***) Regional-mean deviation. (***C***) Network-level reassignment profiles. For each intrinsic network (x-axis), adherence (or 1-deviation) is depicted as the portion of the bar (connecting network) with the equivalent color. All other colors codify exactly which connecting networks were being preferred (see Table 1 and Methods for computation of deviation) when deviating from the predefined partition. That is to say, deviation in (A) is expanded in (C) to show frequency of reassignments, across task states (i.e., affinities). (***D***) The same as in (C), but the x-axis is depicted at the regional level (i.e., these regional reassignments were averaged to generate C).

Next, we performed planned contrasts of control networks' deviation scores versus each other networks' deviation scores, using the max-T method to correct for multiple comparisons (see Materials and Methods). Deviation estimates of FPN regions were significantly different from about half of the

other networks (using the max-T approach, $p<0.0001$), including: secondary visual, somatomotor, cingulo-opercular, auditory, posterior multimodal, ventral multimodal, and orbito-affective. The CON's deviation was significantly higher than every other network (using the max-T approach, $p<0.0001$), except for the orbito-affective network. A paired-samples t-test comparing the deviation of FPN and CON regions revealed a significant difference ($t(49)=6.28$, $p<0.00001$), suggesting that the control networks differ on how often they deviate from their intrinsic partitions across task states. In the *replication* dataset, CON regions' deviations scores were significantly higher than each other network (with no exceptions) (Extended Data Fig. 6-1). Lastly, the paired samples t-test to compare the deviation of CON and FPN in the *replication* dataset likewise showed a significant difference ($t(49)=9.13$, $p<0.00001$).

To further explore the task-state reconfiguration property that deviation was capturing, we generated "reassignment profiles" at both the network (Fig. 6C) and region (Fig. 6D) levels. Reassignment profiles showed precisely which networks were preferred when a region was deviating from the intrinsic partition. As shown in Fig. 6C, the CON deviated to many other networks in an evenly-distributed manner (relative to other networks' reconfigurations) with some bias to somatomotor connections, whereas the FPN deviated less overall and with more specific preferences, favoring the dorsal attention, language, and default networks (in addition to itself). These reconfiguration preferences were consistent in the *replication* dataset profiles, as seen in Extended Data Figures 6-1C and 6-1D. As with other graph metric results, deviation estimates highly overlapped between discovery and replication datasets (*Rho*=0.958, $p<0.00001$), as did reassignment profiles (*Rho*=0.848, $p<0.0001$) (Extended Data Fig. 6-1).

Network Cartographies

We found that FPN regions expressed high GVC and NF (in an optimized sector of the NF parameter space), yet relatively low deviation. CON regions, however, displayed lower GVC and NF, yet higher deviation. Altogether, the CON and the FPN exhibited high reconfiguration properties. However, the diversity of findings across network metrics suggested that composite, multidimensional profiles were warranted to fully map out their functionalities. Careful examination of network metric estimates for CON and FPN regions clarified the pattern of results. FPN connectivity was globally diverse (tending to deviate to specific networks, as in Fig. 6C & 6D), whereas CON connectivity was globally uniform (or "evenly" deviating, as in Fig 6C & 6D). Figure 7A depicts prominent network properties in a cartographic manner (Guimerà and Nunes Amaral 2005; Mattar et al. 2015), charting GVC on the y-axis against deviation on the x-axis. The FPN can be found in the upper right quadrant of this cartography, near the mean demarcation line for deviation (the vertical gray line, Fig. 7A), pointing to the high-variability, yet low-deviation, performance of FPN regions in response to cognitive control task state changes. The CON can be found in the lower right quadrant of the cartography in Fig. 7A, suggesting a low-variability, yet high-deviation, complement to FPN in properties supporting cognitive control.

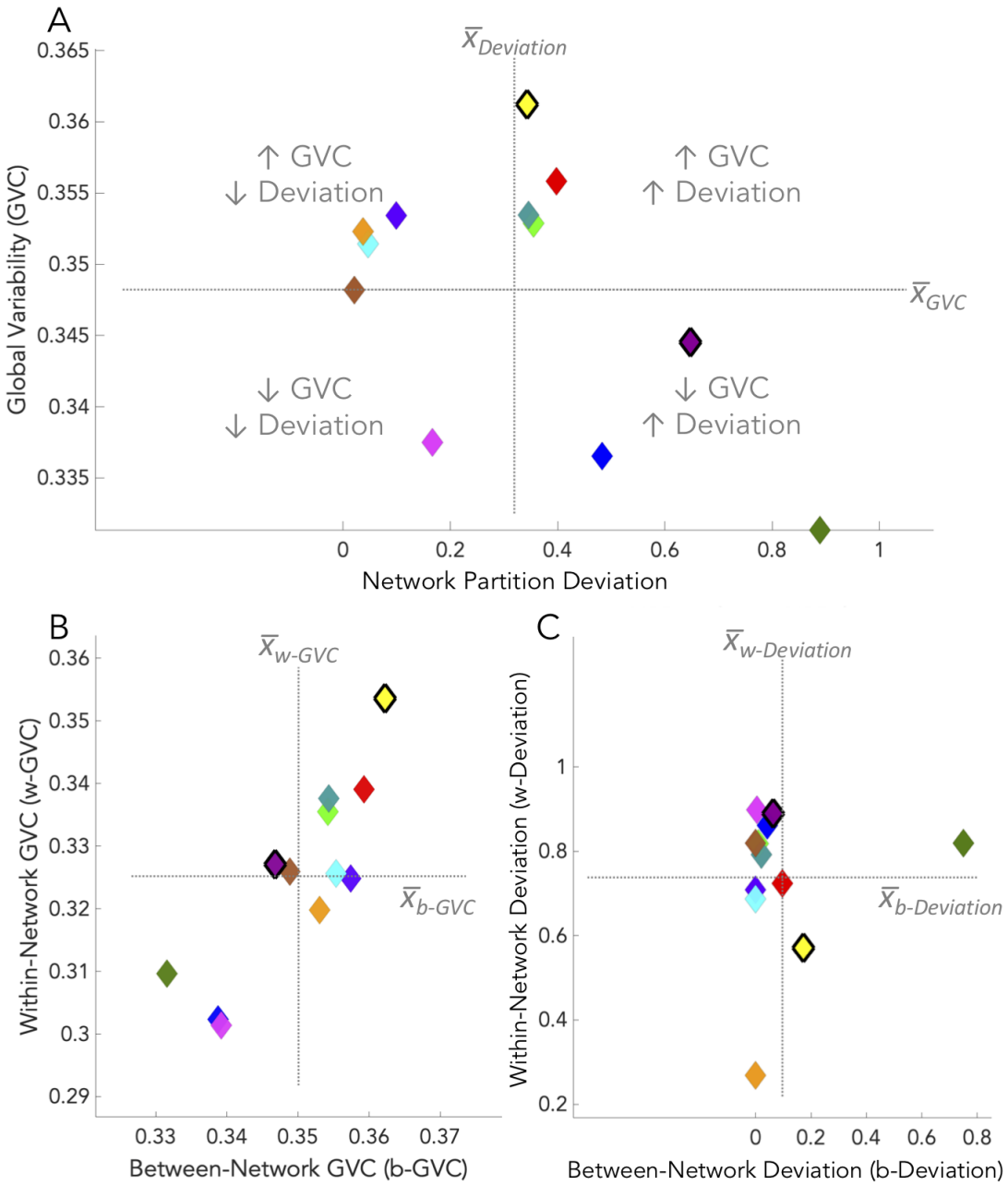

Figure 7. Cognitive control cartographies. (***A***) GVC (as in Fig. 4A) plotted over deviation (as in Fig. 6A), with demarcation lines (dashed and crossed gray lines) indicating the cross-network mean for each dimension (all axes are centered at these marks for ease of viewing). This allowed us to "map out" multidimensional properties at once. For example, networks in the lower right quadrant of A (such as CON) exhibit GVC lower than the mean and deviation higher than the mean. This mapping suggests a nonlinear relationship between GVC and deviation, suggesting that each measure characterizes a unique network property. In all panels, control networks (FPN: yellow, CON: plum) are highlighted with dark black outlines. (***B***) GVC scores (y-axis of panel A) expanded by within-network and between-network values. (***C***) Deviation (x-axis of panel A) scores expanded by within-network and between-network values.

To expand upon the primary mapping in Fig. 7A, we generated two secondary cartographies that depict the quantification of each primary measure's within-network and between-network scores (see Materials and Methods). Briefly, within-network dynamics were assessed by keeping the between-network connectivity fixed across states (defined by resting state). Similarly, between-network dynamics were assessed by keeping the within-network connectivity fixed across states (defined by resting state)

(see Extended Data Fig. 7-2 for data input schematics). Figure 7B charts these dimensions of GVC, showing both within-network and between-network FPN connections to be high on global variability, and CON to be near-mean on within-network GVC and low on between-network GVC. Figure 7C depicts within- and between-network deviation. Both FPN and CON regions were near the mean for between-network deviation (yet on opposing sides of the mean, see vertical gray line in Fig. 7C), yet low and high, respectively, for within-network deviation. This suggests that CON's high deviation was driven primarily by changes in within-network connectivity.

We used paired-samples t-tests to directly compare FPN and CON regions on each secondary cartographic metric (Fig. 7B and 7C), and found the following: (1) FPN was significantly higher than CON on within-network GVC ($t(49)=8.92$, $p<0.00001$); (2) FPN was significantly higher than CON on between-network GVC ($t(49)=11.43$, $p<0.00001$); (3) CON was significantly higher than FPN on within-network deviation ($t(49)=6.55$, $p<0.00001$); and (4) FPN was significantly higher than CON on between-network deviation ($t(49)=4.88$, $p=0.000012$) (see prior results sections for FPN versus CON comparisons on GVC and deviation scores related to Fig. 7A, where all regions were included). This pattern of results replicated in the *replication* dataset: 1) FPN was significantly higher than CON on within-network GVC ($t(49)=8.65$, $p<0.00001$); (2) FPN was significantly higher than CON on between-network GVC ($t(49)=10.26$, $p<0.00001$); (3) CON was significantly higher than FPN on within-network deviation ($t(49)=6.16$, $p<0.00001$); and (4) FPN was significantly higher than CON on between-network deviation ($t(49)=2.13$, $p=0.03$) (Extended Data Fig. 7-1C and 7-1D).

To explore this result further, we created a color-coded graph of the partition reassignments captured by each version of deviation (Fig. 8). To quantify the relationships between reassignment patterns we used the Jaccard similarity index (see Materials and Methods). We found FPN's between-network deviation (i.e., within-network connectivity held constant) was more similar to "all-data" deviation than its within-network deviation (i.e., between-network connectivity held constant): Jaccard indices of 0.29 and 0.18, respectively. Yet, CON's within-network deviation was more similar to "all-data" deviation than its between-network deviation (Jaccard indices of 0.31 and 0.16, respectively). Across subjects, the Jaccard similarity indices for CON and FPN were significantly different (Jaccard for deviation all-data and deviation within-network data, CON vs FPN: $t(49)=3.30$, $p=0.0018$; Jaccard for deviation all-data and deviation between-network data, CON vs FPN: $t(49)=-4.61$, $p=0.00003$). This further demonstrates a dissociation between the cognitive control networks, the CON and the FPN. This supports the conclusion that the high deviation exhibited by the CON was driven by its within-network connections, indicating that CON task-related dynamics were driven mostly by reduction in within-network intrinsic connectivity (network "disbanding") to increase the strength of between-network connections relative to (now-reduced) within-network connections. In contrast, FPN regions maintained their within-network connection patterns while varying their between-network connection patterns across rest and task. This is consistent with FPN maintaining its intrinsic within-network connectivity while reconfiguring its between-network connections in a task-specific manner. Moreover, the pattern of CON within-network decreases were task-specific, as shown in Figure 4E and Figure 8A. This is consistent with CON being a flexible hub network like FPN, but with a distinct mechanism involving "releasing" out-of-network connectivity via dynamic reduction of within-CON connectivity.

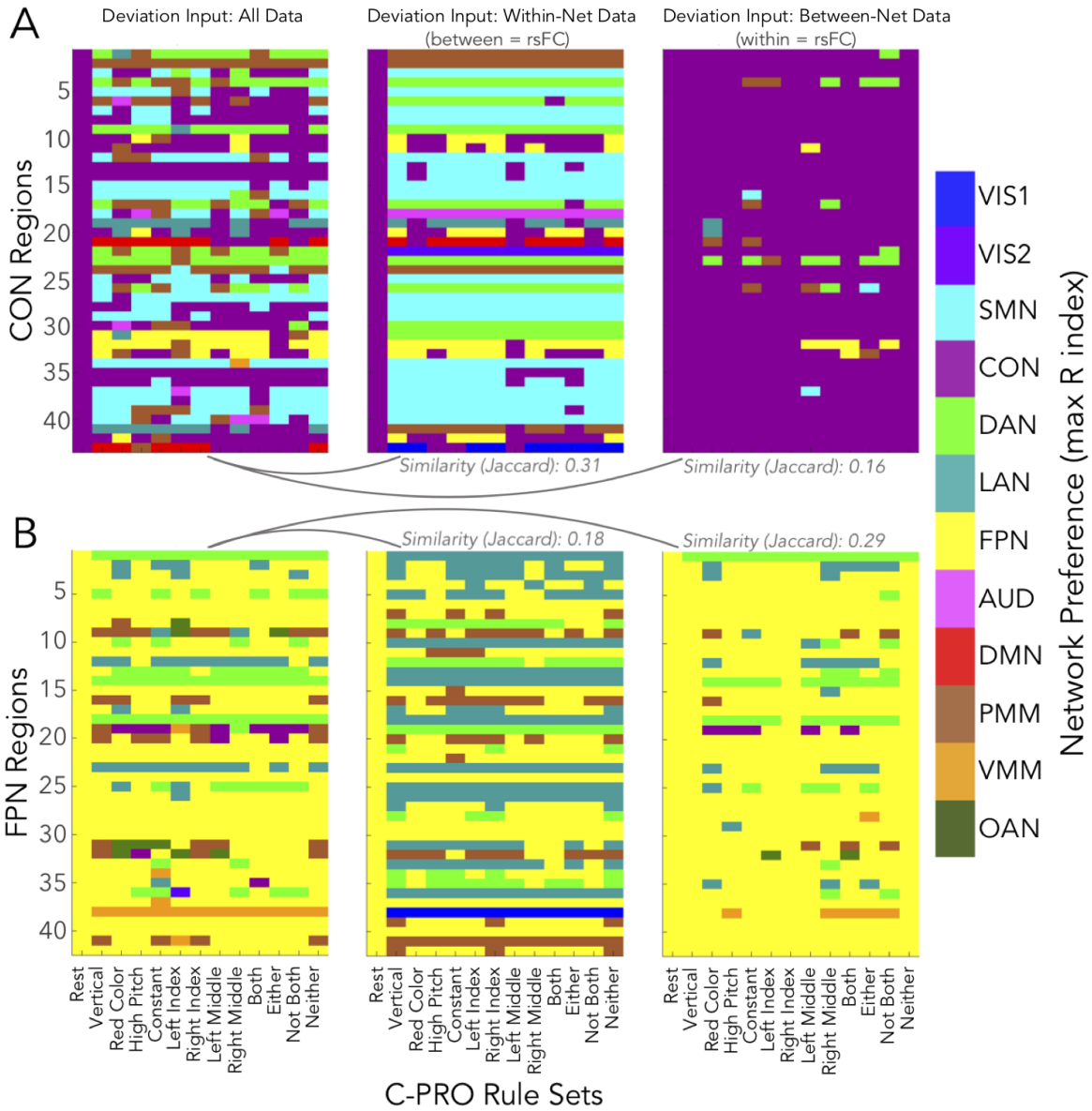

Figure 8. Reassignments conferred by the variants of network partition deviation in the control cartographies. Reassignment is the network index (based on the intrinsic partition) of the highest mean connectivity estimate (see Materials and Methods), per task state. In each panel, Jaccard indices are listed to indicate similarity between two partitions. Network assignments are color coded (as in Fig. 3D), and the 64 C-PRO task states are collapsed into 12 rule sets (plus Rest as a reference on each x-axis). (***A***) *Left*: Network reassignments of CON regions from the deviation algorithm, with all connectivity data included in the input (Fig. 7A, x-axis). *Middle*: Within-network CON estimates used in the deviation algorithm (Fig. 7C, y-axis; Extended Data 7-2C). The Jaccard similarity of within-network and all-data deviation is 0.31. *Right*: Between-network CON estimates used in the deviation algorithm (Fig. 7C, x-axis; Extended Data 7-2D). The Jaccard similarity of between-network and all-data deviation is 0.16, which is lower than the within-network similarity to all-data. (***B***) Same as panel A, except for FPN regions. The Jaccard similarity scores are: within-to-all=0.18, between-to-all=0.29. Thus, FPN showed the reverse pattern to CON, where between-network deviation is more similar to all-data deviation than within-network deviation.

Taken together, the cartographies indicated that CON regions were not maintaining their intrinsic partition during tasks (however, it was not completely lost, given that adherence (1 - deviation) was 0.35). Considering that CON regions switched to other networks with a relatively uniform distribution (across tasks and switched-to networks) (Fig. 4, Fig. 5, & Fig. 6C), and high network partition deviation

across tasks (Fig. 6A), we reasoned that the CON was transiently disbanding, or switching, to lend resources to other goal-relevant networks. Interestingly, FPN regions demonstrated deviation close to the mean of other networks, suggesting that while they do deviate from their partition relative to other networks (a feature essential for cognitive control), their intrinsic organization is still maintained across tasks. Considering that FPN regions exhibited globally diverse flexible hub properties (Fig. 4, Fig. 5, & Fig. 6C) and low deviation across tasks (Fig. 6A), we suggest that the FPN acted as a dynamic global coordinator/integrator of goal-relevant information.

To test if the FPN and CON were statistically distinct across the six measures used in the three cartographies (Fig. 7), we performed a MANOVA (see Materials and Methods) and found that there were statistically significant differences in cartography measures based on control network grouping ($F(5,94)=35.655$, $p<0.00001$, Wilk's $\Lambda=0.35$, $\eta^2=0.65$). MANOVA results were consistent in the replication dataset, likewise showing significant differences in cartography measures based on control network grouping ($F(5,94)=43.007$, $p<0.00001$, Wilk's $\Lambda=0.30$, $\eta^2=0.70$). Altogether, we propose that FPN regions were acting as flexible "coordinators" and CON regions as flexible "switchers", in support of cognitive control (Fig. 9). This cartography of network dynamics reveals a dissociation between two prominent control networks, suggesting complementary, yet distinct, properties underlying goal-directed cognition.

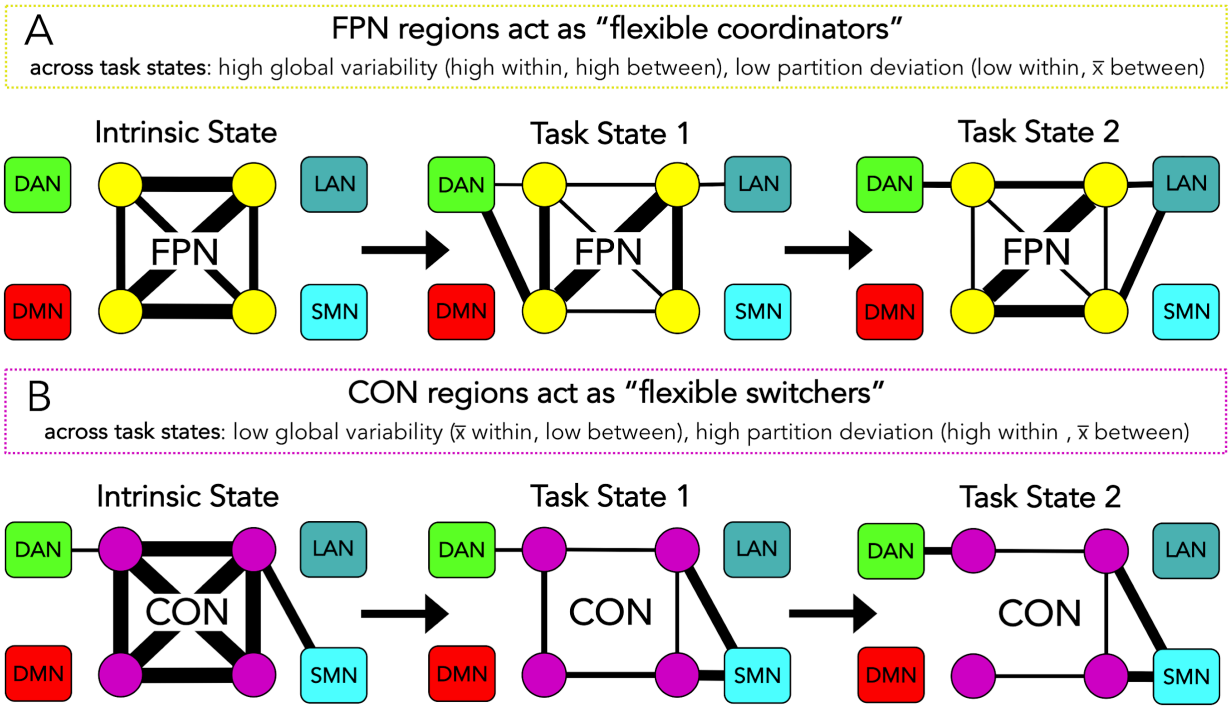

Figure 9. Schematic depictions of cognitive control network functional properties. In each panel, a "toy" version of the control network is prominently depicted in the center (with a reduced number of regions, or nodes, and simplified within-network connections), and out-of-network exemplars are depicted as truncated and surrounding the control network of interest (DAN, LAN, DMN, and SMN). Each of these surrounding networks also contains within-network regions and connections, but these are not depicted here for simplicity. (***A***) Regions in the frontoparietal network (FPN) acted as flexible coordinators. This entailed high global variability and low partition deviation across task states. From example task state one to task state two, FPN regions maintain their within-network connectivity (low deviation) and out-of-network connectivity changes are variable across states (high GVC). (***B***) Regions in the cingulo-opercular network (CON) acted as flexible switchers. This entails low global variability and high partition deviation. From example task state one to task state two, CON regions drop their within-network connectivity (high deviation) and out-of-network connectivity changes are consistent across states (low GVC).

Discussion

The chief conclusion of the current study was that combining network science measures into network cartographies (multi-dimensional "maps" of functionality) allowed us to characterize cognitive control brain systems acting as either flexible coordinators (frontoparietal regions) or flexible switchers (cingulo-opercular regions). The network cartographies consisted of two primary dimensions: 1) GVC, which measures global FC reconfiguration across task states in a continuous manner and, 2) deviation, which measures global FC reconfiguration from rest to task in a discrete manner (Fig. 7). We found that FPN exhibited high GVC but low deviation, while CON showed the opposite pattern, consistent with complementary mechanisms of cognitive control. FPN appeared to act as a "flexible coordinator", based on its extensive between-network FC reconfiguration along with maintenance of within-network FPN connections across rest and task states. In contrast, CON appeared to act as a "flexible switcher", based on CON regions extensively reducing their within-network connections from rest to task to effectively switch to other networks during tasks (Fig. 9).

The present findings are broadly consistent with the view proposed by Dosenbach et al. (2006; 2007; 2008), which posited – based on fMRI task activations and resting-state FC – that control networks implement dissociable mechanisms. We used tFC along with dynamic graph-theoretic measures to expand on Dosenbach et al. In that work, FPN regions enacted control in a manner described as "active, adaptive, and online". The high tFC-based global variability we observed in FPN regions is consistent with adaptive monitoring and adjustment important for controlled processing (see also Cole and Schneider 2007; Sadaghiani and D'Esposito 2015; Crittenden et al. 2016). In contrast to FPN, Dosenbach et al. (2006; 2007; 2008) proposed that CON underlies "stable set maintenance, task mode, and strategy" (also shown by Vaden et al. 2013). While we did find CON connectivity changes to be more consistent (across task states) than FPN (at least in terms of GVC; Fig. 4A), we propose that its functional switching relates to the "biased competition" model put forth by Desimone et al. (1990; 1995) and related theories, as described below.

The biased competition model posits that neural representations compete for resources, such that multiple stimuli, actions, and/or thoughts compete for attention during task performance (Desimone and Duncan 1995). The theory suggests that the competition is biased, however, by top-down goal-related signals from prefrontal cortex and related areas (i.e., control networks). These top-down control signals are thought to shift the competition in bottom-up processing (e.g., in visual cortex), such that goal-relevant processes become more salient and more likely to "win". For instance, a top-down control signal could bias color-naming representations over word-reading representations to aid in Stroop task performance. This theory was built upon by the guided activation theory (Miller and Cohen 2001) and flexible hub theory (Cole et al. 2013b). In line with these later theories, we recently posited that such top-down biases to bottom-up competitive processes are especially important for RITL paradigms (such as the one used here), and that they are implemented by tFC changes from control networks (Cole et al. 2017). The present results suggest top-down biases are implemented via two complementary mechanisms. First, CON regions appear to flexibly switch to other networks in a task-dependent manner, likely lending more "weight" or "energy" to help task-relevant regions/networks win competitions with other regions/networks (or representations). Second, FPN regions appear to flexibly coordinate their global patterns of goal-driven biases with each other via maintaining within-network connectivity. This likely facilitates the coordination of complex task sets via combinations of task rule representations. This account illustrates what appears to be a fundamental trade-off in controlled processing: lending of resources by CON to help goal-relevant brain systems win competitions (e.g., with distracting stimuli), versus implementing goal-relevant "programs" by FPN through coordinated top-down biases.

Interestingly, changes in FPN's between-network connectivity patterns were diverse across FPN regions, but FPN's within-network intrinsic configuration remained intact across task states (Fig. 8 and 9). On the one hand, between-network FC variability corroborates the notion that FPN regions support task-specific coding (Crittenden et al. 2016) and selective attention demands (Sadaghiani and D'Esposito 2015). On the other hand, within-network FC preservation suggests that FPN regions are *coordinating* the FC changes across FPN regions. These dynamics are well-suited to address the "variable binding" problem (Feldman 2013), where variable stimulus information must be linked to task rules to enact cognitive computations. For example, in the presently studied C-PRO paradigm, variable rules must link via logical operations to perform a given task, and variable stimuli must link to those rules to produce correct behavior (Fig. 1). The maintenance of FPN's intrinsic organization combined with between-network reconfigurations (that are diverse from task to task), suggests a coding process that includes FPN, along with other, task-specific regions. This computational format would allow for variable stimulus information to be bound on a task-to-task basis. Specifically, we propose that FPN's role in this scheme is to flexibly coordinate task-specific coding. Notably, this would impose high processing demands on FPN regions, which we suggest to be facilitated by the CON freeing up resources, pointing to a computational trade-off across these two cognitive control networks.

Two other non-control networks joined CON in having low variability and high deviation: the OAN and the primary visual network. Indeed, OAN had both the lowest GVC and the highest deviation of all networks. This suggests that the switching mechanism proposed for CON likely also occurs for OAN, though other studies suggest distinct functionality for OAN. OAN is localized to a small number of regions in a single anatomical cortical location – ventromedial prefrontal cortex (along with nearby subcortical regions) (Ji et al. 2019). Human lesion studies and animal models suggest a core role of OAN in emotion processing and value representation (Roy et al. 2012), and likely receives direct dopaminergic projects from the ventral tegmental area (Seamans and Yang 2004). This role in emotion processing may seem counter to the non-emotional C-PRO paradigm, yet evidence from human lesion studies (Koenigs et al. 2007) and neuroimaging (Botvinick and Braver 2015) demonstrates that decision making involves emotion in the form of motivation biasing competition between outcomes during complex decisions. Future research should assess whether OAN provides a similar mechanism to CON for top-down biasing of cognitive processing, but via an emotional/motivational mode of processing. In contrast to OAN and CON, the primary visual network was not diverse in its connectivity switches, primarily switching to the secondary visual network (extrastriate cortex) (Fig. 6C & D), consistent with integrated visual processing across the two visual networks.

Aside from the high-variability/low-deviation and low-variability/high-deviation cartographic mappings of the FPN and CON, respectively (Fig. 7A), there were two other scenarios possible. First, high-variability and high-deviation across task states: networks exhibiting this profile would have fluctuating connectivity as well as notable partition reassignment from rest to task. The default mode network (red diamond in Fig. 7A) appeared to be the only network trending in this direction. Secondly, low-variability and low-deviation across task states: networks in this quadrant of the cartography would have stable connectivity estimates and adhere to their intrinsic partition. The auditory network was the only observed herein (pink diamond in Fig. 7A), which may relate to sensory regions proposed to have a "rigid core" organization (Bassett et al. 2013b). Other sensory-motor networks also had especially low deviation (compared to cognitive networks), suggesting low vs. high deviation was indicative of sensory-motor vs. cognitive network properties. Future work is warranted to explore this further, particularly if diverse task paradigms are implemented.

An essential consideration for future studies regards the question of timescale. Dosenbach et al. (2007; 2008) found increases in CON activity to be sustained across tasks, while FPN activations were

present at task onset, then adaptively varied with changing task demands. In the present work, we applied network metrics across a set of highly dynamic task states. While measures of global variability summarized the diversity of reconfigurations across states, further examination is required to better determine the timescales of control network mechanisms. Relatedly, future studies would benefit from considering how electrophysiological signatures of neural processing and network properties relate in terms of the instantiation of cognitive control. In resting-state based studies, Sadaghiani et al. (2010; 2012) found distinctions between FPN and CON based on alpha band signatures. Spontaneous activity in CON related to increases in global power, while FPN activity related to increases in long-range phase synchrony. Based on prior electrophysiology literature, these signatures correspond to the functions of tonic alertness and phasic control, respectively. In future work, both rest and task states (paradigms related to cognitive control) should be assessed via alpha band signatures, as well as potential changes in those signatures from rest to task. A potential outcome is that the increases in global power (CON) and long-range synchrony (FPN) would be more apparent from rest to task, constituting another "mappable" reconfiguration property of cognitive control. This would further support the proposition that CON is suited to stably lend processing resources, and FPN to adaptively integrate task-specific information. Moreover, possible interactions between the properties discovered herein (Fig. 7) and electrophysiological properties remains an empirical question.

Taken together, constructing a functional cartography by combining multiple network science measures allowed us to characterize the FPN and CON as complementary systems of cognitive control. We demonstrated that FPN regions enacted control via flexible coordination of reconfiguring connectivity patterns, and CON regions enacted control via flexible switching of network affiliations to lend resources to task-relevant networks. All of these results replicated in a dataset with distinct subjects, and corroborated prior theories that distinct mechanisms of cognitive control are instantiated in parallel via separate large-scale brain systems. Looking forward, we expect the dynamic network neuroscience approach expanded upon here will be effective for functionally characterizing the relationship between neural and cognitive dynamics in other brain systems and other cognitive paradigms.

References

Amelio, A., & Tagarelli, A. (2017). Revisiting Resolution and Inter-Layer Coupling Factors in Modularity for Multilayer Networks. *arXiv [cs.SI]*. Retrieved from http://arxiv.org/abs/1709.07253

Anderson, ML., & Magruder, J. (2017). Split-Sample Strategies for Avoiding False Discoveries. *National Bureau of Economic Research*, Working Papers 23544.

Bassett, DS., Wymbs, NF., Porter, MA., Mucha, PJ., Carlson, JM., & Grafton, ST. (2011). Dynamic reconfiguration of human brain networks during learning. *Proceedings of the National Academy of Sciences of the United States of America*, 108(18), 7641–7646.

Bassett, DS., Porter, MA., Wymbs, NF., Grafton, ST., Carlson, JM., & Mucha, PJ. (2013). Robust detection of dynamic community structure in networks. *Chaos*, *23*(1), 013142.

Bassett, DS., Wymbs, NF., Rombach, MP., Porter, MA., Mucha, PJ., & Grafton, ST. (2013). Task-based core-periphery organization of human brain dynamics. *PLoS Computational Biology*, 9(9), e1003171.

Blair, RC., & Karniski, W. (1993). An alternative method for significance testing of waveform difference potentials. *Psychophysiology*, *30*(5), 518–524.

Botvinick, MM. (2007). Conflict monitoring and decision making: reconciling two perspectives on anterior cingulate function. *Cognitive, Affective & Behavioral Neuroscience*, *7*(4), 356–366.

Botvinick, M., & Braver, T. (2015). Motivation and cognitive control: from behavior to neural mechanism. *Annual Review of Psychology*, *66*, 83–113.

Braun, U., Schäfer, A., Walter, H., Erk, S., Romanczuk-Seiferth, N., Haddad, L., …Bassett, DS. (2015). Dynamic reconfiguration of frontal brain networks during executive cognition in humans. *Proceedings of the National Academy of Sciences of the United States of America*, *112*(37), 11678–11683.

Chein, JM., & Schneider, W. (2012). The Brain's Learning and Control Architecture. *Current Directions in Psychological Science*, *21*(2), 78–84.

Chen, M., Kuzmin, K., & Szymanski, BK. (2015, July 2). Community Detection via Maximization of Modularity and Its Variants. *arXiv* [physics.soc-ph].

Cocchi, L., Zalesky, A., Fornito, A., & Mattingley, JB. (2013). Dynamic cooperation and competition between brain systems during cognitive control. *Trends in Cognitive Sciences*, *17*(10), 493–501.

Cole, MW., Bagic, A., Kass, R., & Schneider, W. (2010). Prefrontal dynamics underlying rapid instructed task learning reverse with practice. *The Journal of Neuroscience: The Official Journal of the Society for Neuroscience*, *30*(42), 14245–14254.

Cole, MW., Bassett, DS., Power, JD., Braver, TS., & Petersen, SE. (2014). Intrinsic and task-evoked network architectures of the human brain. *Neuron*, 83(1), 238–251.

Cole, MW., Braver, TS., & Meiran, N. (2017). The task novelty paradox: Flexible control of inflexible neural pathways during rapid instructed task learning. *Neuroscience and Biobehavioral Reviews*, *81*(Pt A), 4–15.

Cole, MW., Ito, T., Schultz, D., Mill, R., Chen, R., & Cocuzza, C. (2019). Task activations produce spurious but systematic inflation of task functional connectivity estimates. *NeuroImage*, *189*, 1–18.

Cole, MW., Laurent, P., & Stocco, A. (2013). Rapid instructed task learning: a new window into the human brain's unique capacity for flexible cognitive control. *Cognitive, Affective & Behavioral Neuroscience,* 13(1), 1–22.

Cole, MW., Reynolds, JR., Power, JD., Repovs, G., Anticevic, A., & Braver, TS. (2013). Multi-task connectivity reveals flexible hubs for adaptive task control. *Nature Neuroscience*, 16(9), 1348–1355.

Cole, MW., & Schneider, W. (2007). The cognitive control network: Integrated cortical regions with dissociable functions. *NeuroImage*, *37*(1), 343–360.

Cole, MW., Yang, GJ., Murray, JD., Repovš, G., & Anticevic, A. (2016). Functional connectivity change as shared signal dynamics. *Journal of Neuroscience Methods*, *259*, 22–39.

Cole, MW., Yeung, N., Freiwald, WA., & Botvinick, M. (2009). Cingulate cortex: diverging data from humans and monkeys. *Trends in Neurosciences*, *32*(11), 566–574.

Crittenden, BM., Mitchell, DJ., & Duncan, J. (2016). Task Encoding across the Multiple Demand Cortex Is Consistent with a Frontoparietal and Cingulo-Opercular Dual Networks Distinction. *The Journal of Neuroscience: The Official Journal of the Society for Neuroscience*, *36*(23), 6147–6155.

Desimone, R., & Duncan, J. (1995). Neural mechanisms of selective visual attention. *Annual Review of Neuroscience*, *18*, 193–222.

Desimone, R., Wessinger, M., Thomas, L., & Schneider, W. (1990). Attentional control of visual perception: cortical and subcortical mechanisms. *Cold Spring Harbor Symposia on Quantitative Biology*, *55*, 963–971.

Dosenbach, NUF., Fair, DA., Cohen, AL., Schlaggar, BL., & Petersen, SE. (2008). A dual-networks architecture of top-down control. *Trends in Cognitive Sciences*, 12(3).

Dosenbach, NUF., Fair, DA., Miezin, FM., Cohen, AL., Wenger, KK., Dosenbach, RA. T., …Petersen, SE. (2007). Distinct brain networks for adaptive and stable task control in humans. *Proceedings of the National Academy of Sciences of the United States of America*, *104*(26), 11073–11078.

Dosenbach, NUF., Visscher, KM., Palmer, ED., Miezin, FM., Wenger, KK., Kang, HC., …
Petersen, SE. (2006). A core system for the implementation of task sets. *Neuron*, *50*(5), 799–812.

Fair, DA., Schlaggar, BL., Cohen, AL., Miezin, FM., Dosenbach, NUF., Wenger, K.K., … Petersen, SE. (2007). A method for using blocked and event-related fMRI data to study "resting state" functional connectivity. *NeuroImage*, *35*(1), 396–405.

Feldman, J. (2013). The neural binding problem(s). *Cognitive Neurodynamics*, *7*(1), 1–11.

Fox, MD., Snyder, AZ., Vincent, JL., Corbetta M., Van Essen DC., Raichle ME. (2005). The human brain is intrinsically organized into dynamic, anticorrelated, functional networks. *Proceedings of the National Academy of Sciences of the United States of America*, 102(27), 9673-9678.

Gershon, RC., Wagster, MV., Hendrie, HC., Fox, NA., Cook, KF., & Nowinski, CJ. (2013). NIH toolbox for assessment of neurological and behavioral function. *Neurology*, *80*(11 Suppl 3), S2–S6.

Glasser, MF., Coalson, TS., Robinson, EC., Hacker, CD., Harwell, J., Yacoub, E., … Van Essen, DC. (2016). A multi-modal parcellation of human cerebral cortex. *Nature*, 536(7615), 171–178.

Glasser, MF., Sotiropoulos, SN., Wilson, JA., Coalson, TS., Fischl, JL., Andersson, J., … Jenkinson, M. (2013). The minimal preprocessing pipelines for the Human Connectome Projects. *NeuroImage* 80, 105–124.

Glerean, E., Pan, RK., Salmi, J., Kujala, R., Lahnakoski, J. M., Roine, U., … Jääskeläinen, I. P. (2016). Reorganization of functionally connected brain subnetworks in high-functioning autism. *Human Brain Mapping*, *37*(3), 1066–1079.

Gordon, EM., Laumann, TO., Adeyemo, B., Huckins, JF., Kelley, WM., & Petersen, SE. (2016). Generation and Evaluation of a Cortical Area Parcellation from Resting-State Correlations. *Cerebral Cortex*, *26*(1), 288–303.

Guimerà, R., & Amaral, LAN. (2005). Cartography of complex networks: modules and universal roles*. Journal of Statistical Mechanics*, 2005(P02001), nihpa35573.

Hearne, LJ., Cocchi, L., Zalesky, A., & Mattingley, JB. (2017). Reconfiguration of Brain Network Architectures between Resting-State and Complexity-Dependent Cognitive Reasoning. *The Journal of Neuroscience: The Official Journal of the Society for Neuroscience*, 37(35).

Hwang, K., Shine, JM., & D'Esposito, M. (2017). *Fronto-Parietal Interactions With Task-Evoked Functional Connectivity During Cognitive Control*. *bioRxiv*. Retrieved from https://doi.org/10.1101/133611

Ito, T., Brincat, SL., Siegel, M., Mill, RD., He, BJ., Miller, EK., … Cole, MW. (2019). Task-evoked activity quenches neural correlations and variability in large-scale brain systems (p. 560730). https://doi.org/10.1101/560730

Ito, T., Kulkarni, KR., Schultz, DH., Mill, RD., Chen, RH., Solomyak, LI., & Cole, MW. (2017). Cognitive task information is transferred between brain regions via resting-state network topology. *Nature Communications*, 8(1), 1027.

Ji, J. L., Spronk, M., Kulkarni, K., Repovš, G., Anticevic, A., & Cole, M. W. (2019). Mapping the human brain's cortical-subcortical functional network organization. *NeuroImage*, *185*, 35–57.

Koenigs, M., Young, L., Adolphs, R., Tranel, D., Cushman, F., Hauser, M., & Damasio, A. (2007). Damage to the prefrontal cortex increases utilitarian moral judgements. *Nature*, *446*(7138), 908–911.

Krienen, FM., Yeo, BTT., & Buckner, RL. (2014). Reconfigurable task-dependent functional coupling modes cluster around a core functional architecture. *Philosophical Transactions of the Royal Society of London. Series B, Biological Sciences*, *369*(1653).

Mantel, N. (1967). The detection of disease clustering and a generalized regression approach. *Cancer Research*, *27*(2), 209–220.

Marcus, D.S., Harwell, J., Olsen T., Hodge, M., Glasser, M.F., Prior, F., Jenkinson, M., Laumann, T., Curtiss, S.W., Van Essen, D.C. (2011) Informatics and data mining tools and strategies for the Human Connectome Project. Frontiers in Neuroinformatics 5:4.

Mattar, MG., Cole, MW., Thompson-Schill, SL., & Bassett, DS. (2015). A Functional Cartography of Cognitive Systems. *PLoS Computational Biology*, 11(12), e1004533.

Medaglia, JD., Lynall, ME., & Bassett, DS. (2015). Cognitive network neuroscience. *Journal of Cognitive Neuroscience*, *27*(8), 1471–1491.

Mill, RD., Ito, T., & Cole, MW. (2017). From connectome to cognition: The search for mechanism in human functional brain networks. *NeuroImage*, 160, 124–139.

Miller, EK., & Cohen, JD. (2001). An integrative theory of prefrontal cortex function. *Annual Review of Neuroscience*, 24.

Mucha, PJ., Richardson, T., Macon, K., Porter, MA., & Onnela, JP. (2010). Community structure in time-dependent, multiscale, and multiplex networks. *Science*, 328(5980).

Murphy, K., Birn, RM., Handwerker, DA., Jones, TB., & Bandettini, PA. (2009). The impact of global signal regression on resting state correlations: are anti-correlated networks introduced? *NeuroImage*, *44*(3), 893–905.

Nichols, TE., & Holmes, AP. (2002). Nonparametric permutation tests for functional neuroimaging: a primer with examples. *Human Brain Mapping*, *15*(1), 1–25.

Power, JD., Cohen, AL., Nelson, SM., Wig, GS., Barnes, KA., Church, JA., … Petersen, SE. (2011). Functional network organization of the human brain. *Neuron*, *72*(4), 665–678.

Power, JD., Schlaggar, BL., Lessov-Schlaggar, CN., & Petersen, SE. (2013). Evidence for hubs in human functional brain networks. *Neuron*, 79(4), 798–813.

Roy, M., Shohamy, D., & Wager, TD. (2012). Ventromedial prefrontal-subcortical systems and the generation of affective meaning. *Trends in Cognitive Sciences*, *16*(3), 147–156.

Rubinov, M., & Sporns, O. (2010). Complex network measures of brain connectivity: uses and interpretations. *NeuroImage*, *52*(3), 1059–1069.

Sadaghiani, S., & D'Esposito, M. (2015). Functional Characterization of the Cingulo-Opercular Network in the Maintenance of Tonic Alertness. *Cerebral Cortex*, *25*(9), 2763–2773.

Sadaghiani, S., Scheeringa, R., Lehongre, K., Morillon, B., Giraud, AL., & Kleinschmidt, A. (2010). Intrinsic connectivity networks, alpha oscillations, and tonic alertness: a simultaneous electroencephalography/functional magnetic resonance imaging study. *The Journal of Neuroscience: The Official Journal of the Society for Neuroscience*, *30*(30), 10243–10250.

Sadaghiani, S., Scheeringa, R., Lehongre, K., Morillon, B., Giraud, AL., D'Esposito, M., & Kleinschmidt, A. (2012). α-band phase synchrony is related to activity in the fronto-parietal adaptive control network. *The Journal of Neuroscience: The Official Journal of the Society for Neuroscience*, *32*(41), 14305–14310.

Schneider, W., & Chein, JM. (2003). Controlled & automatic processing: behavior, theory, and biological mechanisms. *Cognitive Science*, *27*(3), 525–559.

Schneider, W., Eschman, A., Zuccolotto, A. E-Prime: User's guide (Psychology Software Incorporated, 2002).

Schneider, W., & Shiffrin, R. M. (1977). Controlled and automatic human information processing: I. Detection, search, and attention. *Psychological Review*, *84*(1), 1–66.

Schultz, DH., Ito, T., Solomyak, LI., Chen, RH., Mill, RD., Anticevic, A., & Cole, MW. (2019). Global connectivity of the frontoparietal cognitive control network is related to depression symptoms in the general population. *Network Neuroscience*. Advance publication.

Seamans, JK., & Yang, CR. (2004). The principal features and mechanisms of dopamine modulation in the prefrontal cortex. *Progress in Neurobiology*, *74*(1), 1–58.

Seeley WW, Menon V, Schatzberg AF, Keller J, Glover GH, Kenna H, Reiss AL, Greicius MD. (2007). Dissociable intrinsic connectivity networks for salience processing and executive control. *J Neurosci*. 27:2349–2356.

Sporns, O., & Betzel, R. (2016). Modular Brain Networks. *Ann. Review of Psychology*, 67, 613-640.

Stokes, MG., Kusunoki, M., Sigala, N., Nili, H., Gaffan, D., & Duncan, J. (2013). Dynamic coding for cognitive control in prefrontal cortex. *Neuron*, *78*(2), 364–375.

Vaden, KI., Jr, Kuchinsky, SE., Cute, SL., Ahlstrom, JB., Dubno, JR., & Eckert, MA. (2013). The cingulo-opercular network provides word-recognition benefit. *The Journal of Neuroscience: The Official Journal of the Society for Neuroscience*, *33*(48), 18979–18986.

Yeo, BTT., Krienen, FM., Sepulcre, J., Sabuncu, MR., Lashkari, D., Hollinshead, M., … Buckner, RL. (2011). The organization of the human cerebral cortex estimated by intrinsic functional connectivity. *Journal of Neurophysiology*, *106*(3), 1125–1165.

Yeo, BTT., Krienen, FM., Eickhoff, SB., Yaakub, SN., Fox, PT., Buckner, RL., … Chee, MWL. (2015). Functional Specialization and Flexibility in Human Association
Cortex. *Cerebral Cortex*, *25*(10), 3654–3672.

Zalesky, A., Fornito, A., & Bullmore, E. (2012). On the use of correlation as a measure of network connectivity. *NeuroImage*, *60*(4), 2096–2106.

Extended Data

Table 1-1. Demographic characteristics of the discovery dataset (n=50).

	Male (n=19)				Female (n=31)				
	n	%	mean*	SD (+/-)	n	%	mean*	SD (+/-)	test (male vs female)**
Age (years)			21.16	2.93			19.90	1.64	t(25)=1.71, *p*=0.10
18-24	17	89.47			31	100.00			
25-34	2	10.53			0	0.00			
35-44	0	0.00			0	0.00			
Ethnicity/Race			White	n/a			Black	n/a	χ^2 (5, N=50)=6.29, *p*=0.18
American Indian or Alaskan Native	0	0.00			0	0.00			
Asian	5	26.32			10	32.26			
Black or African American	3	15.79			12	38.71			
Hispanic or Latino	4	21.05			2	6.45			
Native Hawaiin or Pacific Islander	0	0.00			0	0.00			
White or Caucasian	7	36.84			6	19.35			
Other	0	0.0			1	3.23			
Education			student	n/a			student	n/a	χ^2 (2, N=50)=1.27, *p*=0.26
Some college/Associate's degree	15	78.95			28	90.32			
College/Graduate degree	4	21.05			3	9.68			
Not reported	0	0.00			0	0.00			

Summary of the demographic characteristics of the discovery dataset (n=50). There were no significant differences between identified genders on the distributions of age, ethnicity, or education.
* The measure of center used for categorical variables was the mode. 'Student' refers to 'some college'.
** Testing significant differences between males and females. Age: this was a two-sample t-test (adjusted for unequal sample sizes); Ethnicity/race and education: this was a chi-square test of independence.

Table 1-2. Demographic characteristics of the replication dataset (n=50).

	Male (n=25)				Female (n=25)				
	n	%	mean*	SD (+/-)	n	%	mean*	SD (+/-)	test (male vs female)**
Age (years)			25.00	5.35			23.16	3.52	t(48)=1.44, *p*=0.16
18-24	12	48.00			17	68.00			
25-34	10	40.00			8	32.00			
35-44	3	12.00			0	0.00			
Ethnicity/Race			Asian	n/a			Asian	n/a	χ^2 (5, N=50)=7.23, *p*=0.30
American Indian or Alaskan Native	3	12.00			0	0.00			
Asian	8	32.00			10	40.00			
Black or African American	5	20.00			3	12.00			
Hispanic or Latino	1	4.00			4	16.00			
Native Hawaiin or Pacific Islander	0	0.00			0	0.00			
White or Caucasian	7	28.00			8	32.00			
Other	1	4.00			0	0.00			
Education			graduate	n/a			student	n/a	χ^2 (2, N=50)=1.47, *p*=0.48
Some college/Associate's degree	9	36.00			12	48.00			
College/Graduate degree	13	52.00			12	48.00			
Not reported	3	12.00			1	4.00			

Summary of the demographic characteristics for the replication dataset (n=50). All table features are the same as Extended Data Table 1-1. Note that there were no significant differences between identified genders on the distributions of age, ethnicity, or education.

Table 3-1. Similarities of resting-state FC and multitask FC.

C-PRO Rule-Set	Correlation with Rest (*Mantel-r*)	Shared Variance (R^2)
Sensory rules		
Vertical orientation	0.7966	0.6346
Red color	0.7918	0.6269
High pitch sound	0.7964	0.6343
Constant tone	0.7864	0.6184
Motor rules		
Left index finger	0.7847	0.6158
Right index finger	0.7966	0.6346
Left middle finger	0.7939	0.6303
Right middle finger	0.7844	0.6153
Logic rules		
Both	0.7983	0.6373
Either	0.7934	0.6295
Not both	0.7833	0.6136
Neither	0.7966	0.6346

Relationships between intrinsic rsFC and tFC estimates via Mantel-r (see Fig. 3 and Materials and Methods). In each case (table row), task states comprising tFC estimates (used in each comparison to rsFC) were based on each of the 12 C-PRO rules (see Fig. 1), and averaged across n=50 participants. Connectivity of all C-PRO rule sets significantly correlated with rsFC.

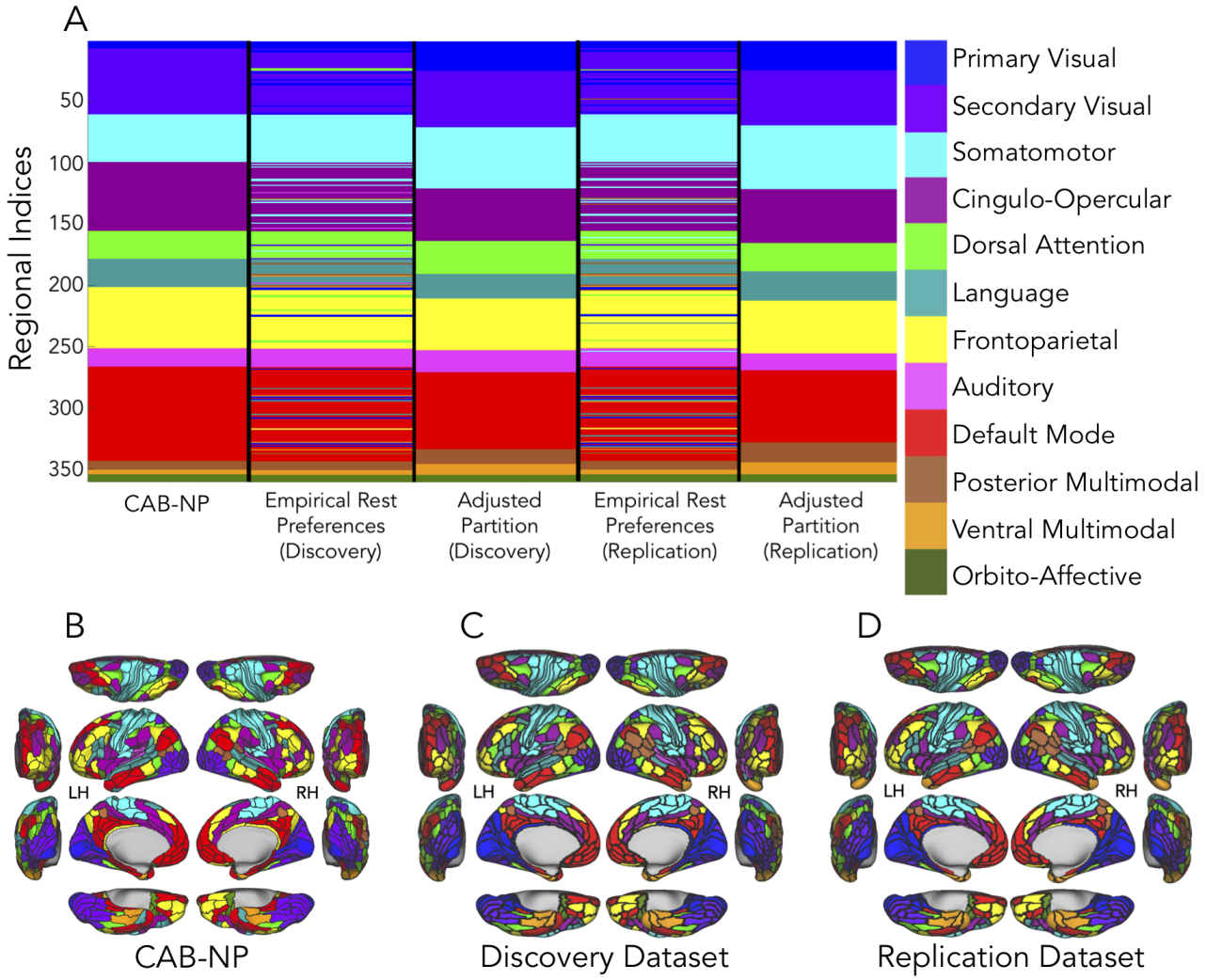

Figure 3-1. The Cole-Anticevic brain-wide network partition (CAB-NP) adjusted by empirical resting-state FC (Fig. 3A), for both the discovery dataset (n=50) and the replication dataset (n=50). (***A***) Regional (y-axis; Glasser et al. 2016 parcels) assignments are color-coded according to the CAB-NP (rightmost scale; and as in Fig. 3D). The CAB-NP column depicts the original resting-state network partition by Ji et al. 2019. The empirically-derived rest preferences are shown, unordered, for both the discovery and replication datasets, as well as their ordered counterparts (i.e., "adjusted partitions"). These adjusted partitions were used for all analyses (see Materials and Methods for details). (***B***) CAB-NP by Ji et al. (2019) projected onto brain regions. (***C***) The empirically-adjusted CAB-NP for the discovery dataset projected onto brain regions. (***D***) The empirically-adjusted CAB-NP for the replication dataset projected onto brain regions. The Jaccard similarity coefficient between discovery and replication partitions was 0.9595, suggesting the partition method used herein will have high external validity.

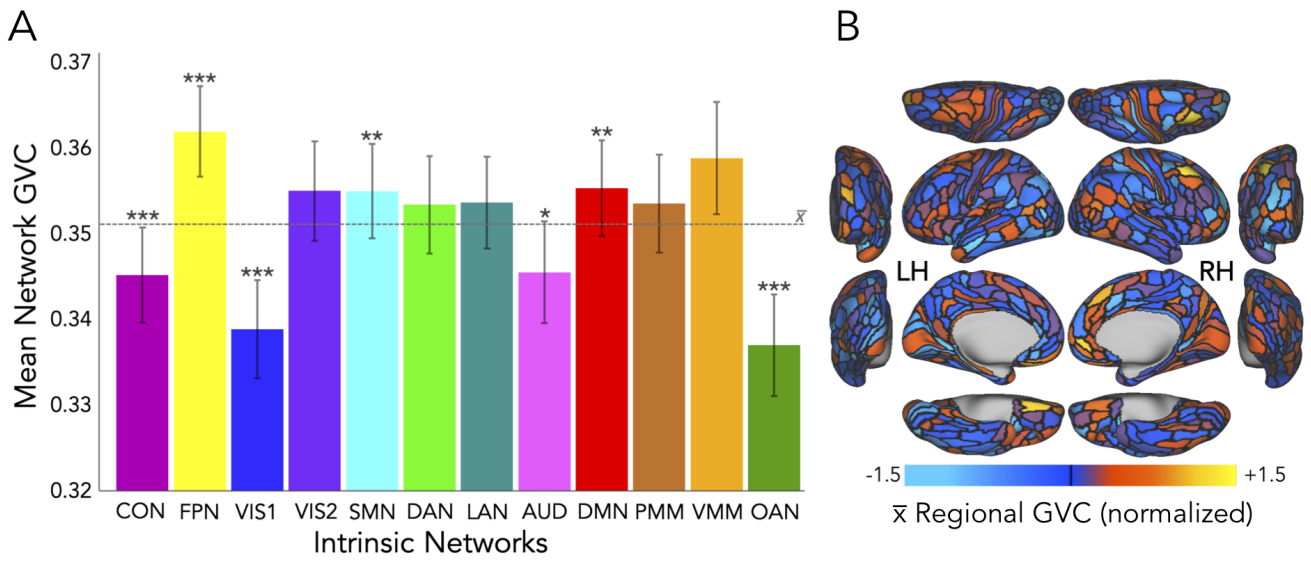

Figure 4-1. Global variability coefficient (GVC), replication dataset. (***A-B***) Panels are represented exactly as in Fig. 4, except measurements were taken for the replication dataset (n=50). GVC results highly overlapped between discovery and replication datasets: *Rho*=0.9091, *p*<0.00001.

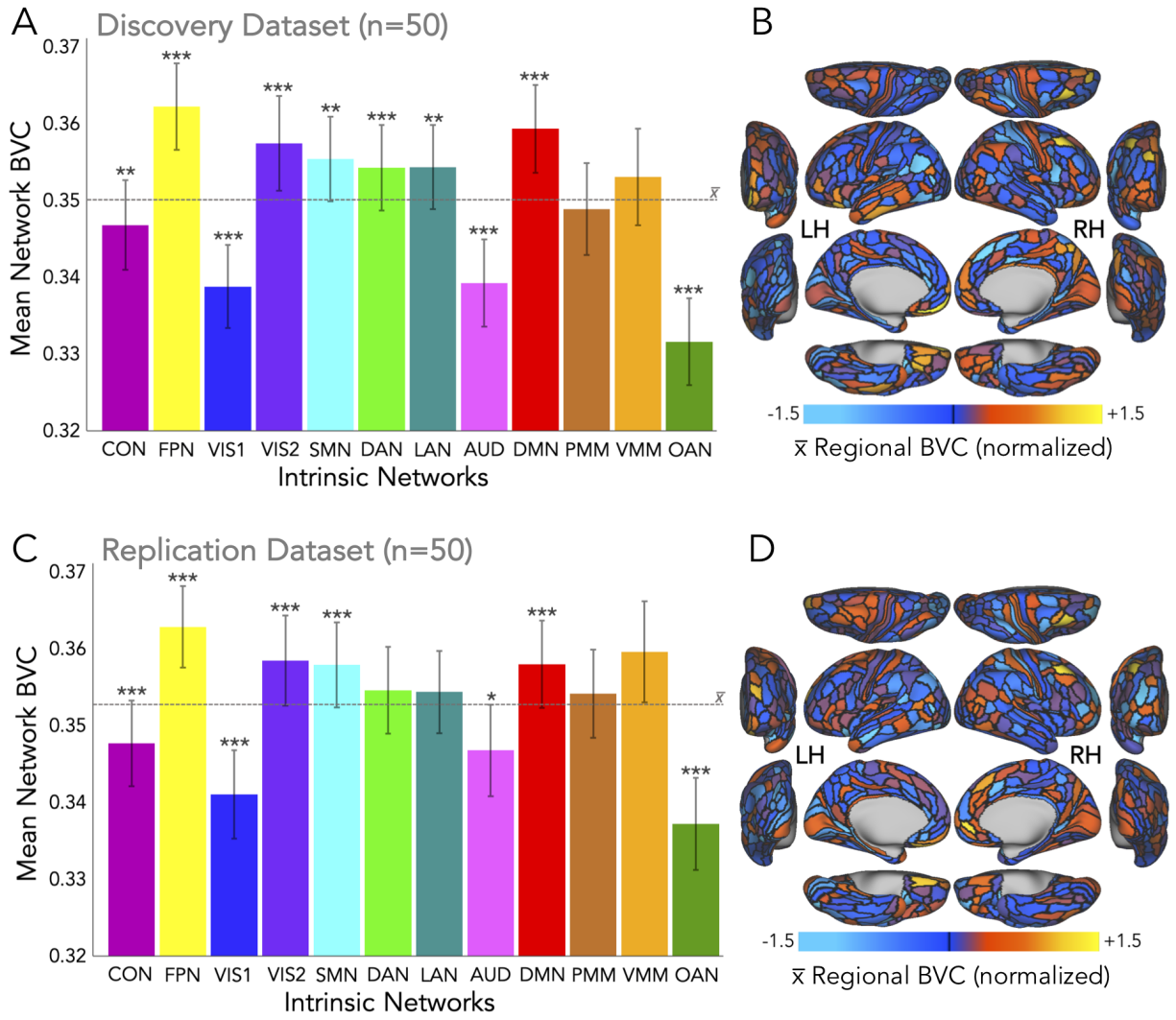

Figure 4-2. Between-network variability coefficient (BVC). (***A-B***) Panels are represented exactly as in Fig. 4, except BVC scores are shown (discovery dataset, n=50). (***C-D***) Same as in A-B, except for the replication dataset (n=50). BVC results highly overlapped between discovery and replication datasets: *Rho*=0.881, *p*=0.0002.

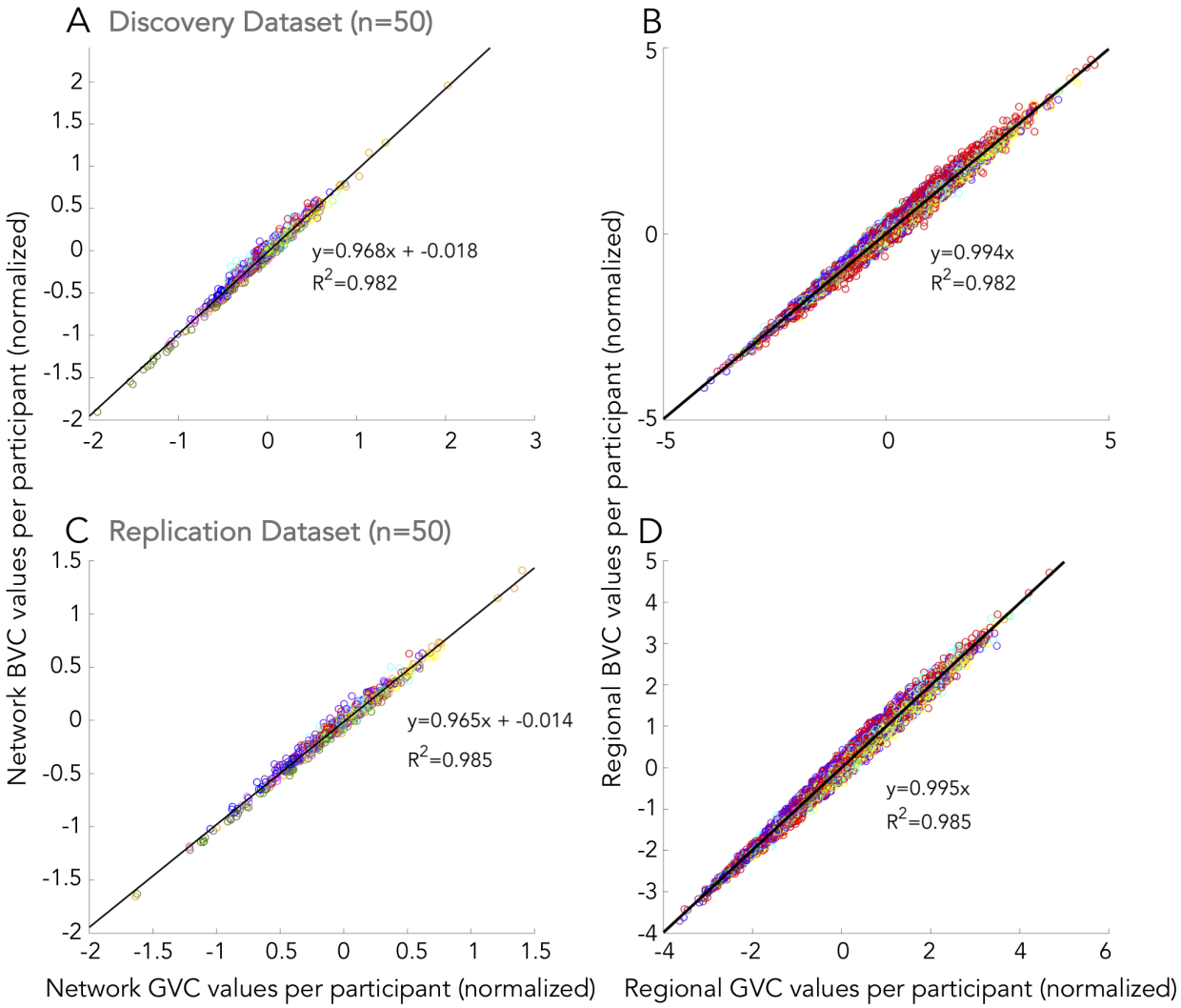

Figure 4-3. Linear relationships between GVC and BVC. In each panel, circles represent individual participant's scores (i.e., what was averaged in Fig. 4), color-coded for network assignments (as in Fig. 3D). Slope-intercept formulae are listed ($y = mx + b$), along with shared variances (R^2). At all levels of measurement and for both discovery and replication sets, GVC and BVC were highly correlated. (***A***) Discovery dataset (n=50) and network-level scores. (***B***) Discovery dataset and regional-level scores. (***C***) Replication dataset (n=50) and network-level scores. (***D***) Replication dataset and regional level scores.

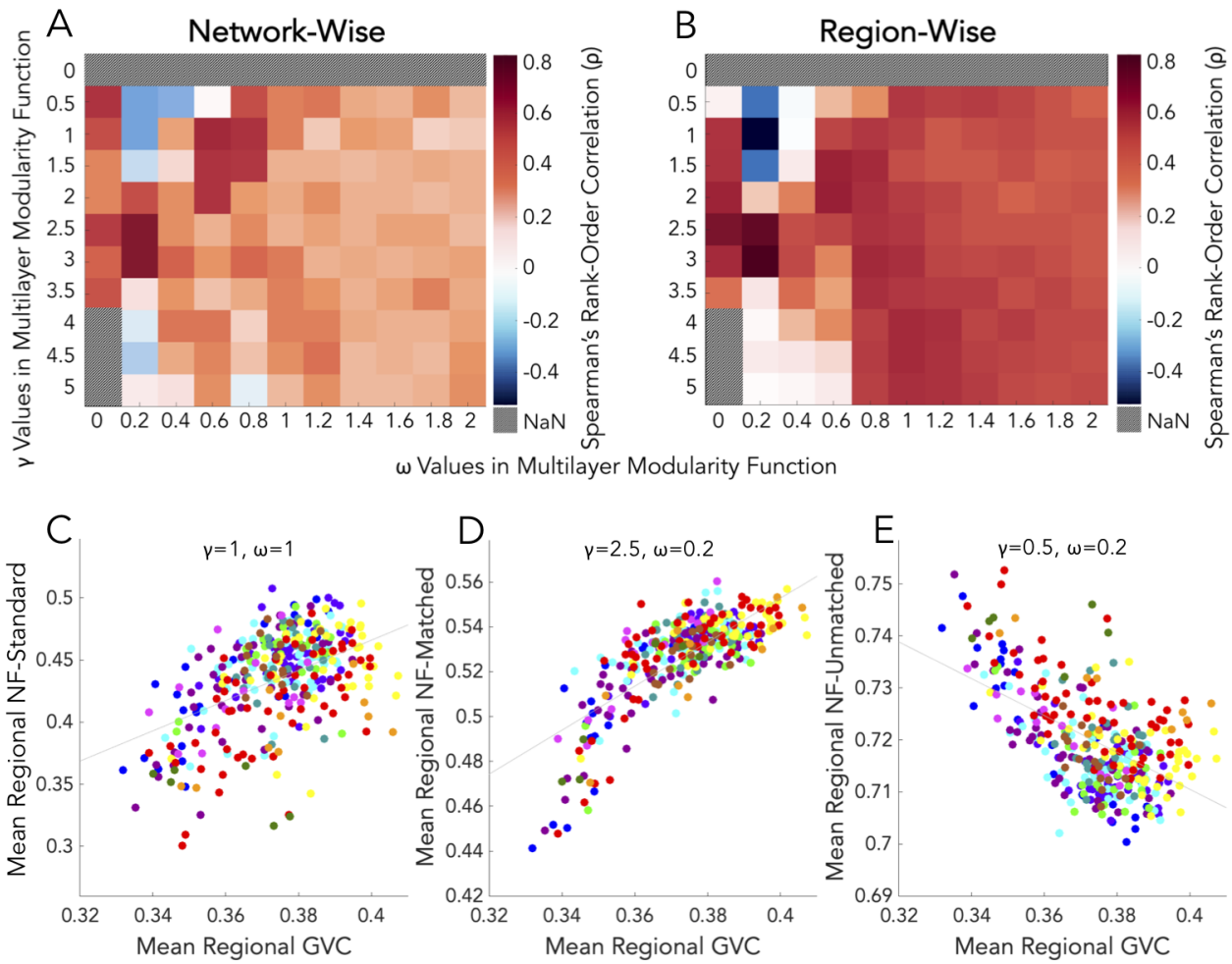

Figure 5-1. Comparison of NF and GVC, replication dataset. (***A-F***) Panels are represented exactly as in Figure 5 (discovery dataset, n=50), except measurements were taken for the replication dataset (n=50). Note that the parameter combination utilized for NF-standard (γ=1 and ω=1) (panel C) was the same as in Fig. 5C because this was based on the literature-standard. The parameter combinations used in the multilayer modularity function yielding NF-matched (panel D) and NF-unmatched (panel E) were set to the same values as in Fig. 5 even though there were higher and lower Rho values in the region-wise comparison with GVC for the replication set (panel B), respectively. More specifically, the regional NF vector most similar to GVC was yielded by γ=3 and ω=0.2 in the replication dataset, as opposed to γ=2.5 and ω=0.2 in the discovery dataset. However, γ=2.5 and ω=0.2 did yield the highest Rho value in the network-wise comparison with GVC (panel A) in the replication set, thus we continued to use this combination for NF-matched as it lead to the highest similarity score in most analyses. The same rationale was applied to NF-unmatched, where the parameter combination of γ=0.5 and ω=0.2 was used.

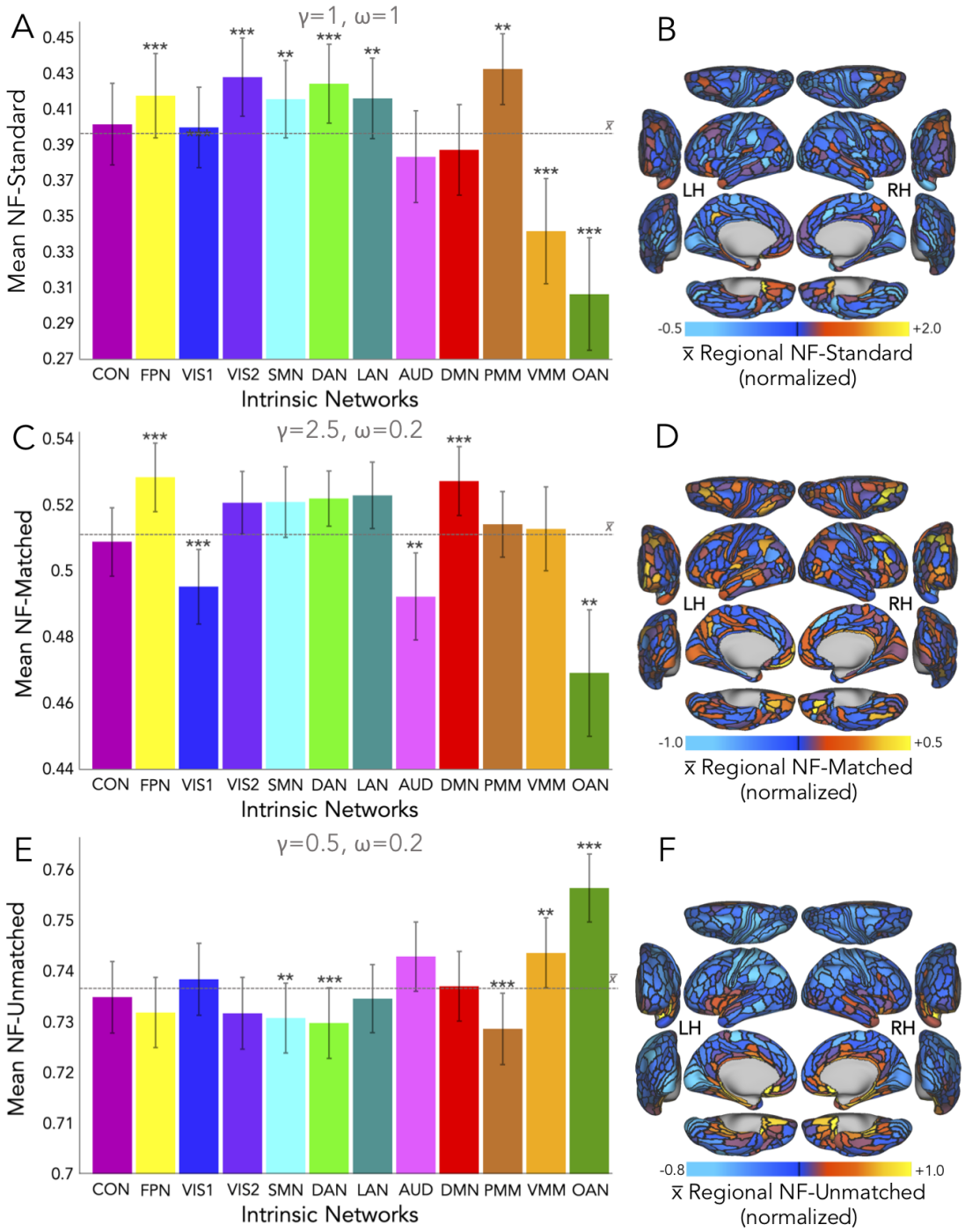

Figure 5-2. Network Flexibility (discovery dataset, n=50). Mean, SEM, and hypothesis testing specifications are the same as in Fig. 4. (***A***) Network-mean NF-standard, where γ=1 and ω=1. (***B***) Regional-mean NF-standard. (***C***) Network-mean NF-matched, where γ=2.5 and ω=0.2 and correlation with GVC was highest. (***D***) Regional-mean NF-matched. (***E***) Network-mean NF-unmatched, where γ=0.5 and ω=0.2 and correlation with GVC was lowest. (***F***) Regional-mean NF-unmatched. Note that NF results results highly overlapped between discovery and replication datasets. NF-standard: *Rho*=0.9301, *p*<0.00001; NF-matched: *Rho*=0.7133, *p*=0.012; NF-unmatched: *Rho*=0.9021, *p*<0.00001.

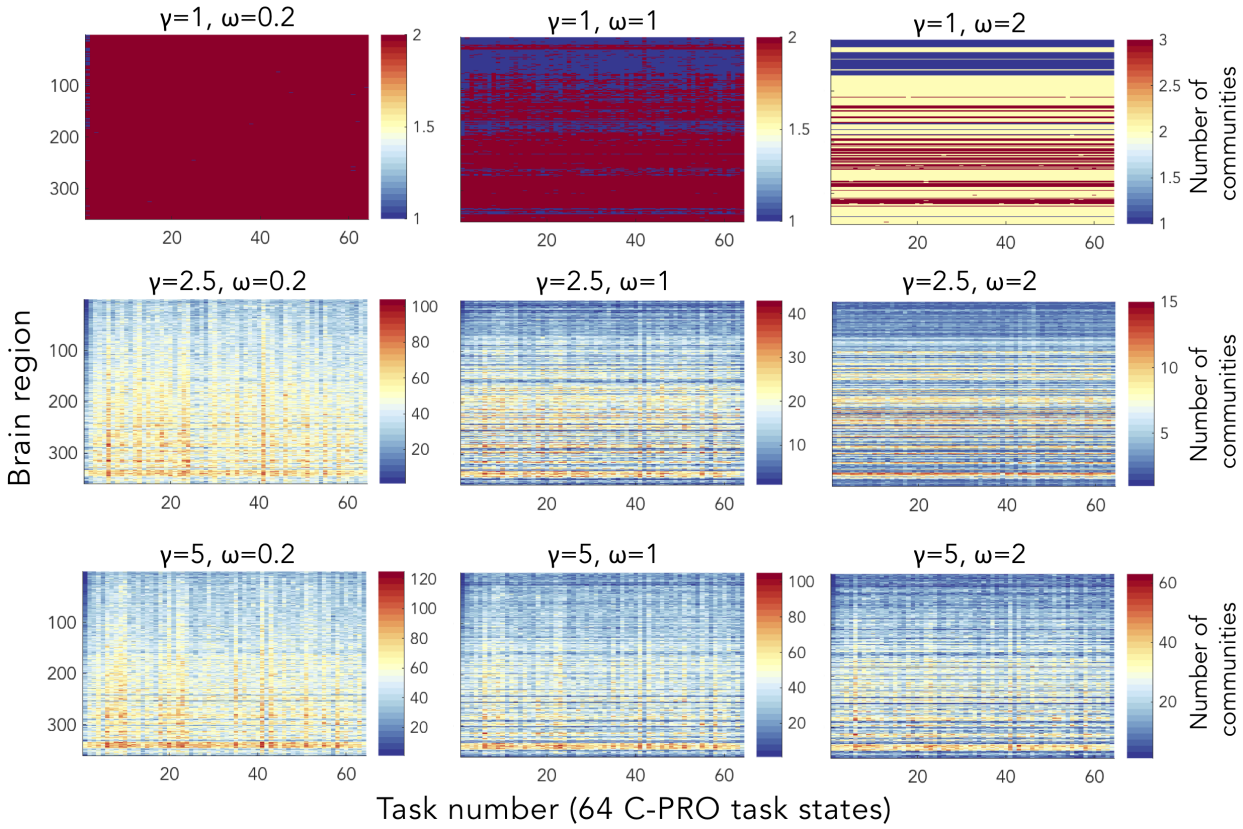

Figure 5-3. Network assignment structures resolved by the multilayer community detection algorithm required for network flexibility (Fig. 5), swept by ranges of spatial resolution (γ) and temporal resolution (ω) parameters. Each square depicts the average number of communities (averages were across participants; number of communities are color-coded by corresponding scales), for each region (y-axis) and each C-PRO task state (x-axis). These assignments were used in the computations of NF, except at the individual participant level. Discovery dataset (n=50) is depicted here. For simplicity, low, medium, and high parameter values are illustrated (the entire parameter space constituted an 11 by 11 matrix, as in Fig. 5A & 5B). NF-standard (Fig. 5C & 5D), where γ=1 and ω=1, was yielded by the community assignments summarized in the top-middle square. This parameter combination tended to generate an undersized number of communities. NF-matched (Fig. 5E & 5F), where γ=2.5 and ω=0.2, was yielded by the community assignments summarized in the left-middle square. We propose that the higher spatial resolution (γ=2.5 versus γ=1) captured a near-continuous distribution of connectivity estimates, creating many small networks. GVC also treats connectivity data as spatially continuous via use of first- and second-moment statistics (Fig. 2A), which partially accounts for the high correlation between NF-matched and GVC. The smaller temporal resolution in NF-matched (ω=0.2 versus ω=1) further accounts for this high correlation by slightly offsetting the spatial resolution and keeping the 64 task states from merging into one large state.

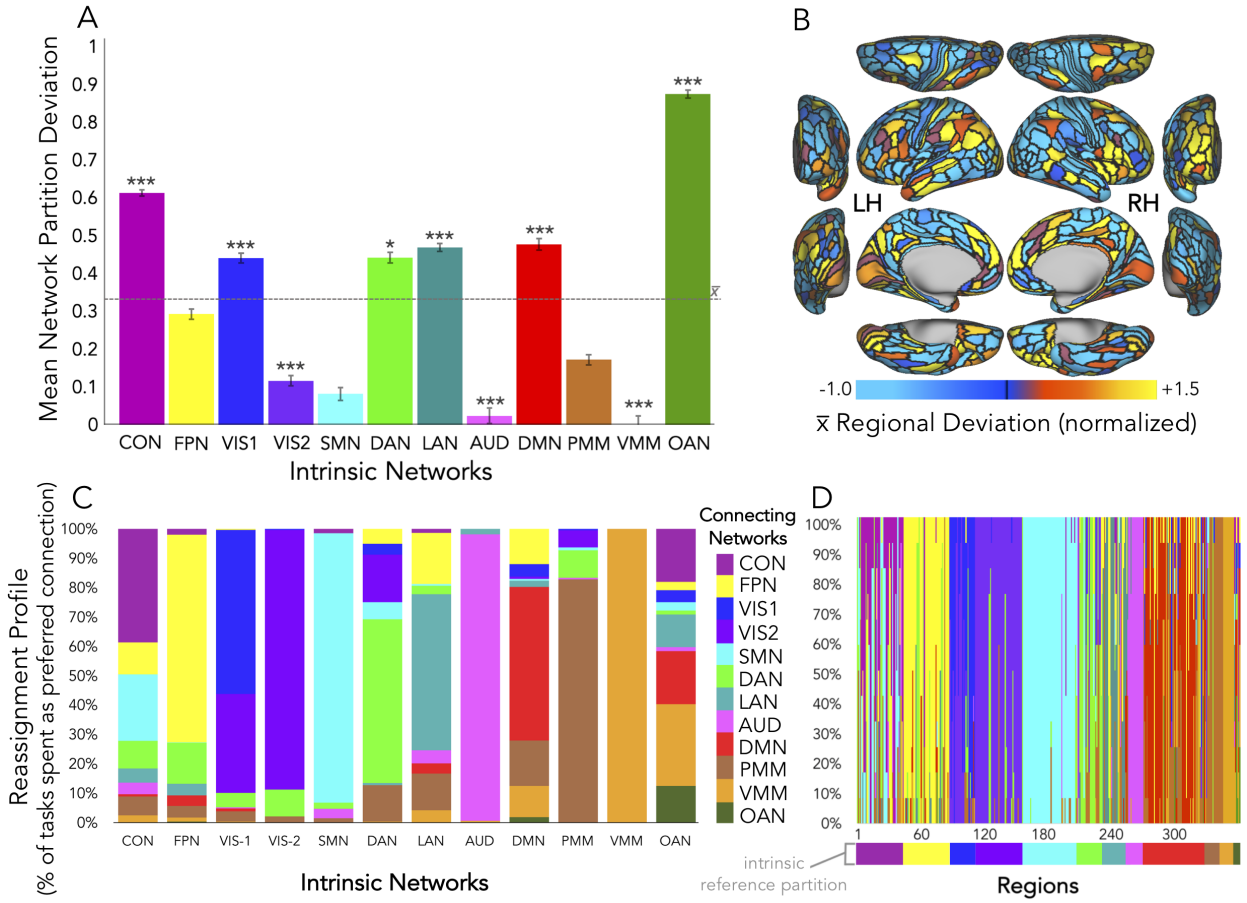

Figure 6-1. Network partition deviation and reassignment profiles, replication dataset. (***A-D***) Panels are represented exactly as in Fig. 6, except measurements were taken for the replication dataset (n=50). Deviation results (panels A) highly overlapped between discovery and replication datasets: *Rho*=0.9580, *p*<0.00001. Network reassignment profiles (panels C) also corresponded: *Rho*=0.8477, *p*<0.0001.

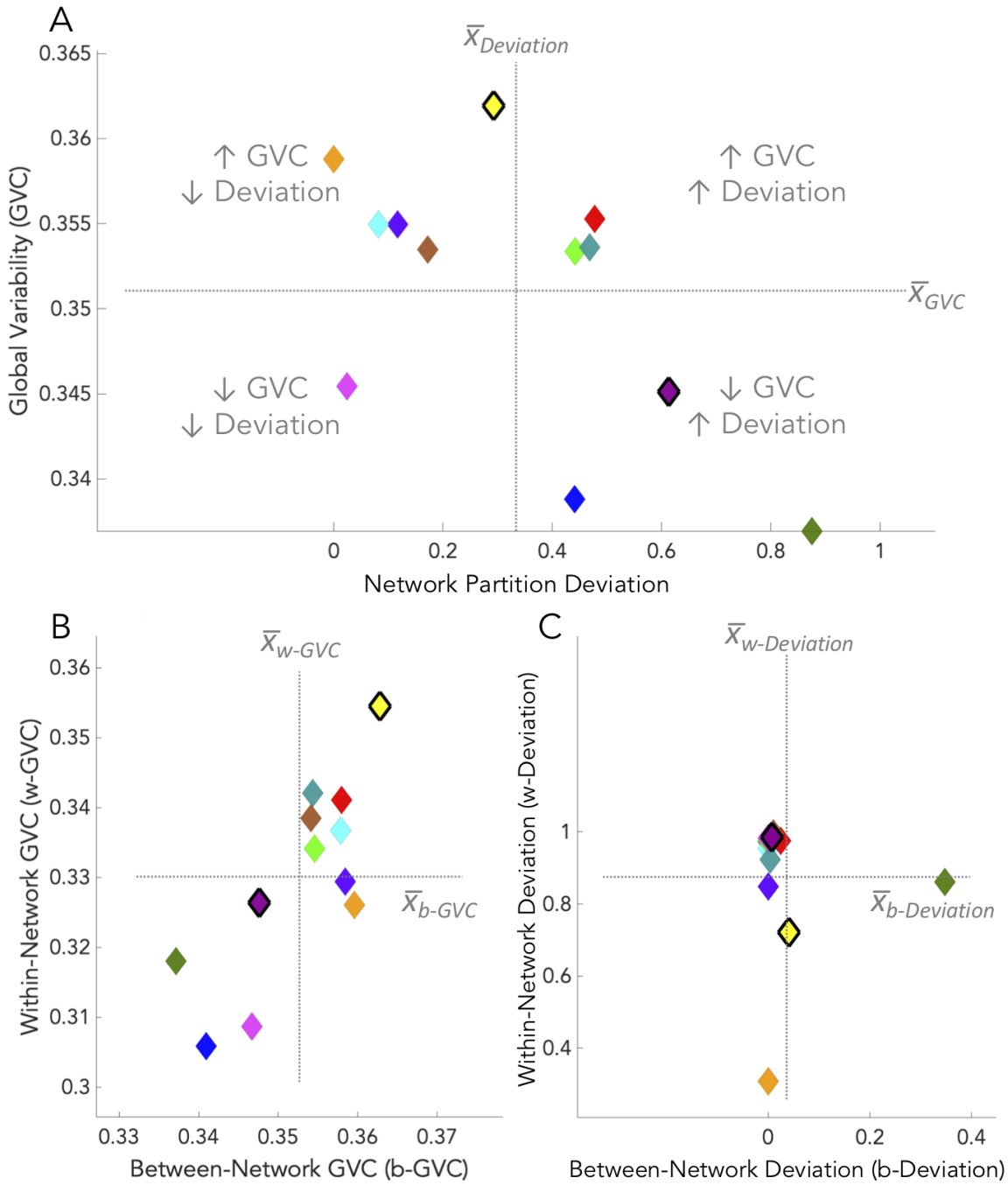

Figure 7-1. Cognitive control cartographies, replication dataset. (***A-C***) Panels are represented exactly as in Fig. 7, except measurements were taken for the replication dataset (n=50). All measures highly overlapped between discovery and replication datasets: GVC: *Rho*=0.9091, *p*<0.00001; Deviation: *Rho*=0.9580, *p*<0.00001; within-network GVC: *Rho*=0.9091, *p*<0.00001; between-network GVC: *Rho*=0.881, *p*=0.0002; within-network Deviation: *Rho*=0.7566, *p*=0.004; between-network Deviation: *Rho*=0.7162, *p*=0.008. Moreover, the MANOVA results were replicated, wherein the six cartographic measures were significantly different based on control network grouping ($F(5,94)=43.007$, $p<0.00001$, Wilk's $\Lambda=0.30$, $\eta^2=0.70$).

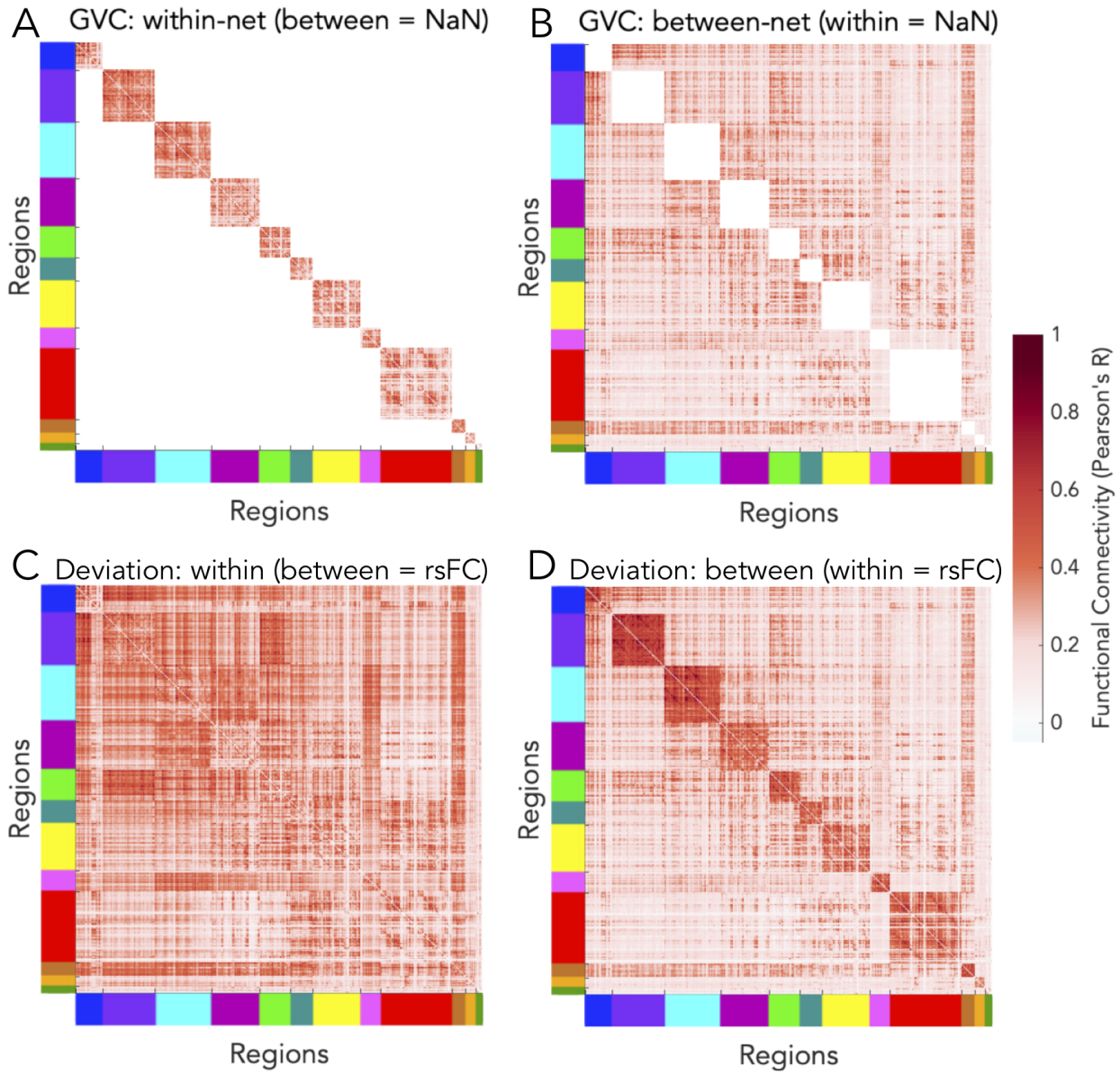

Figure 7-2. Input data schemes used in computing measures of the secondary cognitive control cartographies (Fig. 7B & 7C). Data refers to functional connectivity estimates (Pearson's R; colored according to the right-most scale). Put another way, each panel contains modified adjacency matrices. The cross-state means are visually represented, but analyses included all 64 C-PRO task states. Axes are color coded according to the empirically-adjusted CAB-NP (see Fig. 3C and Extended Data Fig. 3-1). (***A***) Representation of input data for within-network GVC (Fig. 7B, y-axis). Between-network FC estimates were set to 'NaN' (white). (***B***) Input data for between-network GVC (Fig. 7B, x-axis). Within-network FC estimates were set to 'NaN' (white). (***C***) Input data for within-network deviation (Fig. 7C, y-axis). Between-network FC estimates were set to their resting-state values. (***D***) Input data for between-network deviation (Fig. 7C, x-axis). Within-network FC estimates were set to their resting-state values.

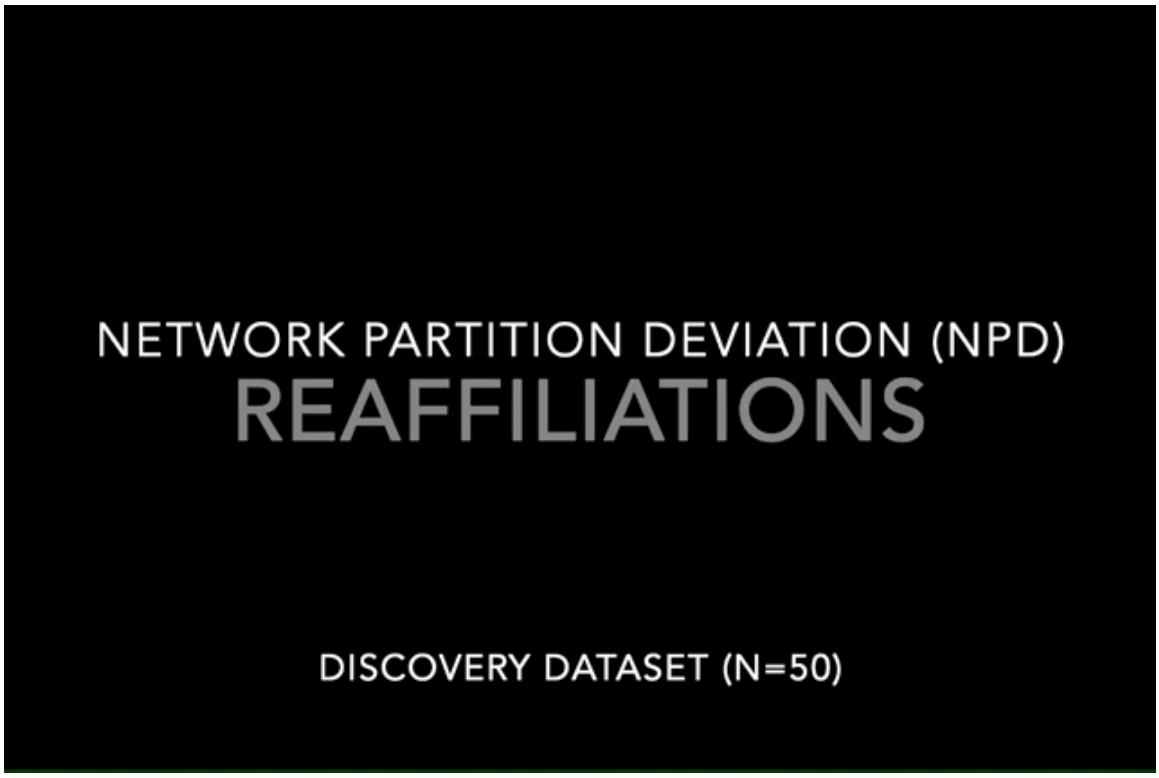

Multimedia 1. Video of each region's network "preference" observed during the computation of network partition deviation, across all 64 C-PRO task states, and for n=50 discovery dataset participants (see Materials and Methods). Briefly, per task state and region, the maximum connectivity estimate was found, and its location relative to the predefined partition (empirically adjusted CAB-NP) was indexed (see Fig. 2 & Table 1). These network indices were then mapped back onto brain schematics to visualize how deviation defines network reassignment across tasks. This video also depicts the dynamics captured by deviation. Some patches of cortex remained stable in their network assignments across states (such as primary and secondary visual networks, shown mainly in occipital regions as blue and purple, respectively). However, some regions and/or networks reassigned with more frequency, such as as the shifts in cingulo-opercular preference observed in diverse regions. The goal of deviation was to quantify these patterns in a systematic manner. Cortical regions on each brain schematic represent the Glasser parcellation scheme (2016), and colors correspond to the CAB-NP naming system (Ji et al. 2019) (see Fig. 3).